UNIVERSITÄT
LEIPZIG

Temperature-Dependent Photoluminescence of MgV, GeV and NV Color Centers in Diamond for Thermometry Applications

Master Thesis

ENA OSMIĆ

Supervisors
Prof. Dr. Jan Meijer
Dr. Sébastien Pezzagna

University of Leipzig
Faculty of Physics and Earth Sciences
Applied Quantum Systems Department
Leipzig, May 2021

Contents

1 Introduction

Temperature is one of the most important parameters of the intracellular environment because it changes the dynamics and the reactivity of biomolecules. Each biological reaction that controls cell functions occurs either exothermically or endothermically in particular microdomains of a cell. Biological reactions cause the release of Gibbs free energy, which triggers cellular functions. The unused energy is transformed into heat, the heat production then elevates the local temperature. Many mechanisms inside the cell, as well as in the extracellular matrix can be responsible for the local temperature increase, as a result, reaction rates are accelerated following the change in chemical equilibria. Therefore, if there exists a heterogeneous temperature distribution within a cell, it may strongly correlate with cell activities via biochemical reaction processes. Fluorescence-based imaging has been the main strategy for intracellular thermometry, because it can be non-invasive and can have a high spatiotemporal resolution compared with a classical calorimetry or infrared thermography. Temperature measurement is achieved by the appropriate combination of thermometric properties and thermosensors. Fluorescence imaging-based thermometry utilizes the temperature dependent change of emission intensity, emission lifetime, or emission wavelength at maximum intensity. These techniques have revealed the temperature distribution or event-driven temperature elevation in a cell.

Diamond implanted with colour centres is an excellent potential candidate for temperature sensing in a delicate environment of a cell, due to its biocompatibility and chemical inertness [21,36]. In recent years, works have been done, researching NV centers as temperature sensors, they possess a thermally sensitive optically detected magnetic resonance (ODMR) signal embedded within a biologically compatible fluorescence band, making them effective thermal probes of living systems that are nonetheless limited by the deleterious effect of requisite microwave excitation on living organisms. All optical micro- and nanoscale quantum thermometers based on silicon-, tin-, and germanium-vacancy color centers in diamond have demonstrated excellent temperature resolution and small sensor volumes necessary for accurate, high-resolution in vivo thermometry. One of the reasons is that, e.g., GeV centers emit a high fraction of fluorescence into the zero-phonon line (ZPL).

Aim of this works is the production of NV, GeV and MgV centers inside the bulk diamond. NV and GeV will be used as a reference and comparison with previous literature results and as a test for the newly designed and self-

built temperature stage. The Magnesium Vacancy is new recently reported color center [12], structure of it is still unknown, whether it is a divacancy, trivacancy etc., remains to be discovered. A main goal of this Master work is to show if the MgV can be used as an effective temperature sensor, and to investigate whether it is a better candidate then GeV.

2 Theoretical Background

2.1 Diamond

Diamond, an allotrope of carbon, is commonly associated with sparkling jewellery and gemstones, such as the amazing Dresden Green Diamond (Fig.1), and with the concept of extreme hardness, which originates in its cubic crystal structure.

Figure 1: Dresden Green Diamond [1].

Diamonds have been adapted for many uses because of the material's exceptional physical characteristics. Of all known substances, it is the hardest and least compressible. It has the highest thermal conductivity and the highest sound velocity. It has low adhesion and friction, and its coefficient of thermal expansion is extremely low. Its optical transparency extends from the far infrared to the deep ultraviolet and it has high optical dispersion. It

also has high electrical resistance. It is chemically inert, not reacting with most corrosive substances, and has excellent biological compatibility.

2.1.1 Crystal Structure

Diamond is a solid form of pure carbon with its atoms arranged in a crystal. Solids made of pure carbon come in different forms known as allotropes depending on the type of chemical bond. The two most common allotropes of pure carbon are diamond and graphite. In graphite the bonds are sp^2 orbital hybrids and the atoms form in planes with each bound to three nearest neighbors 120 degrees apart. In diamond they are sp^3 and the atoms form tetrahedra with each bound to four nearest neighbors.

The term "sp^3 hybridization" refers to the mixing character of one 2s-orbital and three 2p-orbitals to create four hybrid orbitals with similar characteristics. In order for an atom to be sp^3 hybridized, it must have an s orbital and three p orbitals.

$$\left|\Psi_{sp^3}^{(1)}\right\rangle = \frac{1}{\sqrt{4}}(|\Psi_{2s}\rangle + |\Psi_{2px}\rangle + |\Psi_{2py}\rangle + |\Psi_{2pz}\rangle \tag{1}$$

$$\left|\Psi_{sp^3}^{(2)}\right\rangle = \frac{1}{\sqrt{4}}(|\Psi_{2s}\rangle + |\Psi_{2px}\rangle - |\Psi_{2py}\rangle - |\Psi_{2pz}\rangle \tag{2}$$

$$\left|\Psi_{sp^3}^{(3)}\right\rangle = \frac{1}{\sqrt{4}}(|\Psi_{2s}\rangle - |\Psi_{2px}\rangle - |\Psi_{2py}\rangle + |\Psi_{2pz}\rangle \tag{3}$$

$$\left|\Psi_{sp^3}^{(4)}\right\rangle = \frac{1}{\sqrt{4}}(|\Psi_{2s}\rangle - |\Psi_{2px}\rangle + |\Psi_{2py}\rangle - |\Psi_{2pz}\rangle \tag{4}$$

Plotting any of these four wave functions gives a picture representation of a sp^3 orbital (Fig. 2).

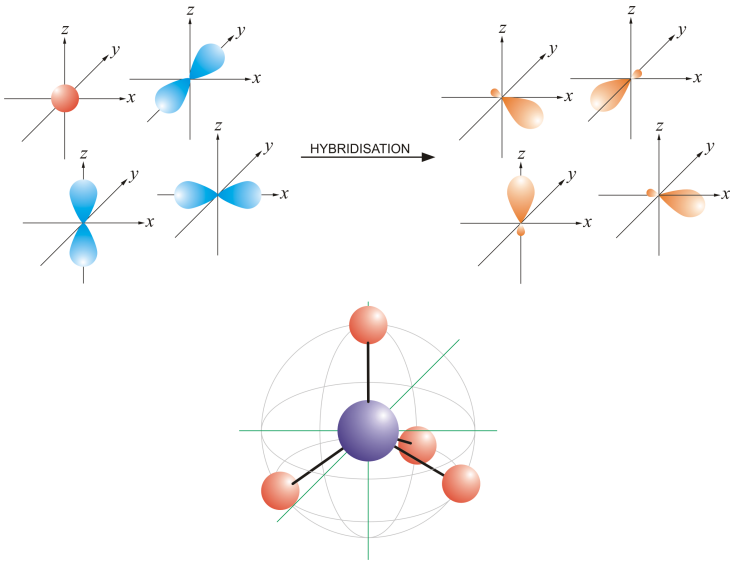

Figure 2: Hybridization of sp^3 orbital [2].

The angle γ between two adjacent hybrid orbitals in the diamond structure is given by the tetrahedral symmetry and amounts to:

$$\gamma = 180^\circ - 2 \arcsin\left(\frac{1}{\sqrt{3}}\right) \approx 109,47^\circ$$

The most common crystal structure of diamond is called diamond cubic. It is formed of unit cells (Fig. 3) stacked together. Although there are 18 atoms in the figure, each corner atom is shared by eight unit cells and each atom in the center of a face is shared by two, so there are a total of eight atoms per unit cell. Each side of the unit cell is 3.57Å in length.

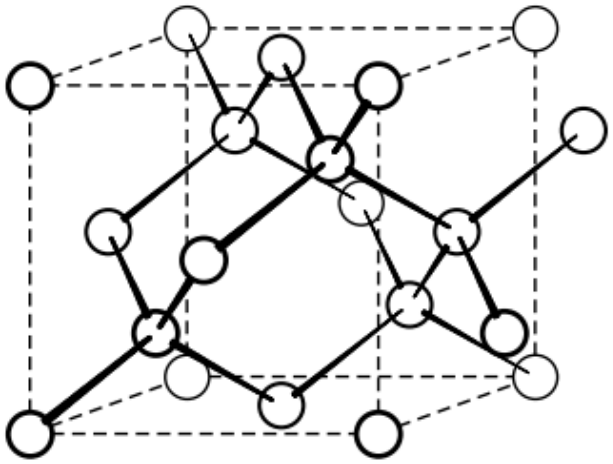

Figure 3: Diamond structure [3].

2.1.2 Electronic Structure

The electronic structure of the diamond is given by its lattice structure. In Figure 4 is shown the electronic band-structure (i.e., dispersion relation) of diamond, which can be described as an fcc lattice with a diatomic basis. Since we want to display a three-dimensional spectrum (energy as a function of k) on a one-dimensional diagram, shown are several single-line cuts through reciprocal space. Starting on the left of the diagram, we start at the L-point of the Brillouin zone and show $E(k)$ as k traces a straight line to the Γ point, the center of the Brillouin zone. Then we continue to the right and k traces a straight line from the Γ point to the X point. Then we make a straight line from X to K and then X back to Γ. Note that the lowest band is quadratic at the center of the Brillouin zone (a dispersion $\hbar k^2/(2m^*)$ for some effective mass m^*).

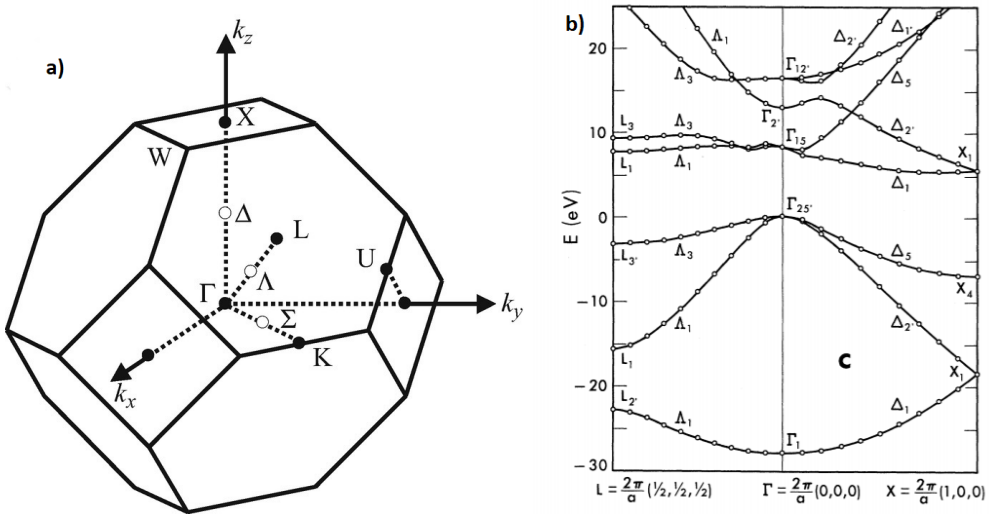

Figure 4: In (a) the first Brillouin zone of the fcc lattice is shown and in (b) the electronic excitation spectrum of diamond. The momentum, along the horizontal axis is taken in straight line cuts between special labeled points in the Brillouin zone. [4]

The upper valence band edge is given by $\Gamma_{25'}$. States, which are energetically higher than $\Gamma_{25'}$, count towards the conduction band. Due to the different possible interband transitions between the valence band edge and the first and second conduction band, the experimental determination of the direct band gap proves to be difficult. Experimental values of the direct band gap are in the range from 6.0 eV to 7.4 eV [52]. The minimum of the conduction band is on the Δ-line for a wave vector $\vec{k}_{min} = (0,76 \pm 0,02) \cdot \vec{k}(X)$ [4]. The indirect band gap at room temperature is given by [4]:

$$E_g(295\text{ K}) = \Gamma_{25'} - \mathrm{E}(\tilde{\mathrm{k}}_{\mathrm{min}}) = 5,470 \pm 0,005\text{ eV} \tag{5}$$

Similarly, in Figure 5, the phonon spectrum of diamond is shown. There are several things to note about this figure. First of all, since diamond has a unit cell with two atoms in it (it is fcc with a basis of two atoms) there should be six modes of oscillation per k-points (three directions of motion times two atoms per unit cell). Indeed, this is what we see in the picture, at least in the central third of the picture. In the other two parts of the picture, one sees fewer modes per k-point, but this is because of the symmetry of the crystal along this particular direction, several excitation modes have exactly

the same energy. Secondly, we note that at the Γ-point, $k = 0$, there are exactly three modes which come down linearly to zero energy. These are the three acoustic modes, the higher one being a longitudinal mode and the lower two being transverse. The other three modes, which are finite energy at $k = 0$, are the optical modes.

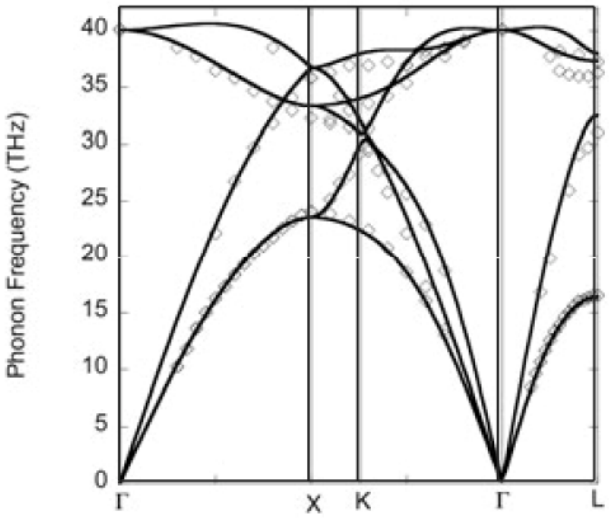

Figure 5: Phonon spectrum of diamond [4].

2.1.3 Optical properties

Optical properties play an important role in the investigation, characterization, and application of diamond. These optical properties have always made diamond so attractive in its natural beauty, and it still keeps its commercial value today. The unique optical properties of diamond are also one of the main criteria for its industrial use, being the second best property after mechanical hardness.

Many outstanding physical properties of diamond make it an attractive material for optical and optoelectronic applications. Diamond has the widest optical transparency band of all known solids, which ranges from 0.22 μm (fundamental absorption edge) to the far-infrared [54]. Only the intrinsic vibrational absorption band of moderate intensity between $2.5 - 7$ μm disturbs the perfection of diamond's transparency in the infrared region. Being

transparent in the ultraviolet, visible and infrared spectral regions, diamond provides many opportunities for lattice defects to reveal the optical activity of their electronic and vibrational transitions. The large bandgap energy (5.47 eV) is a particularly favorable condition in the case of luminescence, because the radiative electronic transitions require that both the ground and excited electronic states lie within the bandgap. The high mechanical hardness and thermal conductivity of diamond greatly support its optical applications making diamond optics very stable and resistant in many respects.

An important optically related feature of diamond is its high Debye temperature (about 2000K). Actually this is the highest Debye temperature of those known for any solids [54]. Owing to the high Debye temperature, a remarkable excitation of phonons in the diamond lattice, and consequent electron-phonon coupling with lattice modes in optically active defects, occurs at elevated temperatures.

The absorption of light in insulating solids (like diamond) arises from two principal sources: electronic transitions and lattice vibrations. Electronic absorption typically occurs in the ultraviolet, whereas absorption by lattice vibrational modes occurs in the infrared. A phonon is a quantum of lattice vibration (elastic) energy (as the photon is the quantum of electromagnetic energy). Phonons are classified as either acoustic (compression waves) or optic. Optical phonons that are infrared active absorb light through an interaction between the electric field of the light and the dipole moment of the material. Diamond is a symmetric, covalent material with no dipole moment and therefore has no infrared active phonons. Weak phonon absorption can be induced in solids by very intense light (Raman-active phonons) or by combinations of phonons (multiphonons) that create weak dipole moments. Diamond has one Raman mode (observed at 1332.4 cm^{-1}) and one acoustic mode [54]. In crystals, frequencies of these modes change with propagation direction, creating many two-phonon absorption features. These multiphonon absorption bands are weak compared with fundamental (one-phonon) absorption and occur at frequencies that are harmonics of the fundamental frequency. In diamond, which has no infrared-active one-phonon absorption, multiphonon effects dominate infrared absorption.

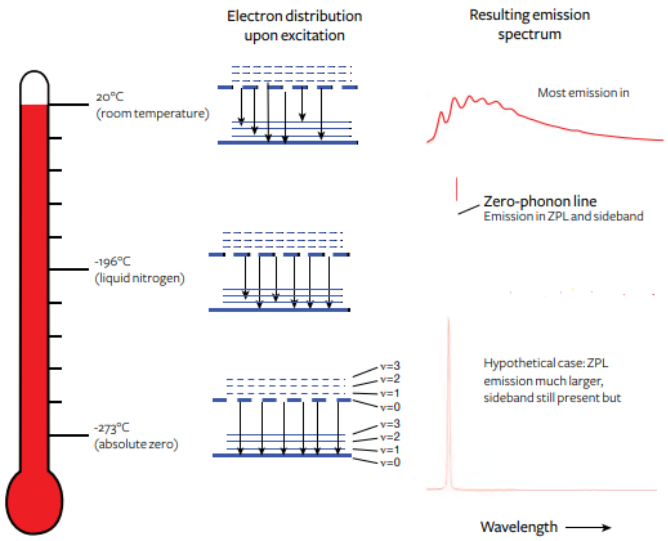

Figure 6: In the hypothetical case of absolute zero temperature, electrons reside at the lowest energy level of the ground state (solid lines), where phonons equal zero. Then they are excited to the level of the "excited" state (dashed lines). This theoretical results in a nearly 100% ZPL emission. As temperature increases to room temperature, electrons are in higher vibrational energy states, creating an ever-increasing distribution of luminescence pathways (black arrows). The resulting emission is spread across a wide wavelength range as a sideband with little to no ZPL emission. [5].

The refractive index n of diamond is given by Sellmeier equation [1]

$$n^2 - 1 = \frac{4.335\lambda^2}{\lambda^2 - (0.1060)^2} + \frac{0.3306\lambda^2}{\lambda^2 + (0.1750)^2} \tag{6}$$

where the wavelength λ is in micrometers. This equation can be used to determine reflectivity from 0.225 μm (in the ultraviolet) through the infrared. Note that diamond has a high index of refraction with high dispersion in the visible (which is enhanced by the cut of diamond gems) and essentially no dispersion in the infrared.

[1]The Sellmeier equation is an empirical relationship between refractive index and wavelength for a particular transparent medium.

2.1.4 Colour Centers in Diamond

Imperfections in the crystal lattice of diamond are common. Such crystallographic defects in diamond may be the result of lattice irregularities or extrinsic substitutional or interstitial impurities, introduced during or after the diamond growth. The defects affect the material properties of diamond and determine to which type a diamond is assigned; the most dramatic effects are on the diamond color and electrical conductivity. When discussing the optical properties of a material its optical centers should be considered carefully, because their properties and abundance determine almost all optical performance of the material. The content of optical centers is the main parameter of the optical characterization of the material. So far more than 150 vibrational and more than 500 electronic optical centers have been detected in diamond within the spectral range of $20 - 0.17$ μm; that is, between the vacuum ultraviolet and the mid-infrared regions.

Both types of intrinsic point defects (vacancy- and interstitial-related) in diamond can form optical centers. Many impurities are known to form optically active defects in diamond: H, He, Li, B, N, 0, Ne, P, Si, As, Ti, Cr, Ni, Co, Zn, Zr, Ag, W, Xe and Tl. Many of the optical centers related to these impurities have been created artificially using doping during growth and, in particular, ion implantation. These centers have never been seen before in pristine natural diamonds. The reason for that is the very short and strong sp^3 hybridized covalent C-C electronic bonds preventing thermodynamical equilibrium (or quasi-equilibrium) incorporation of impurities (even hydrogen) into the diamond lattice. The only remaining possibility is the use of forced methods of impurity insertion, such as ion implantation. Another reason for the high efficiency of the ion implantation as a method of optical activation of diamond is its inevitable creation of radiation damage. Since the majority of optically active defects in diamond are complexes involving impurity atoms bound to some intrinsic structural defects (vacancies and/or interstitial atoms), defect production is an essential advantage of ion implantation.

2.1.5 Nitrogen Vacancy Centers

As stated above, point defects may introduce levels in the fundamental bandgap of semiconductors or insulators that radically change the optical and magnetic properties of the host material. In particular, these point de-

fects could be paramagnetic, i.e. the electron spin is greater than zero. A primary example of such a point defect is the NV center in diamond. The nitrogen-vacancy center is a point defect in the diamond lattice. It consists of a nearest-neighbor pair of a nitrogen atom, which substitutes for a carbon atom, and a lattice vacancy. Nitrogen-vacancy centers are typically produced from single substitutional nitrogen centers (called C or P1) by irradiation followed by annealing at temperatures above 700°C [53]. A wide range of high-energy particles is suitable for such irradiation, including electrons, protons, neutrons, ions, and gamma photons. Irradiation produces lattice vacancies, which are a part of NV centers. Those vacancies are immobile at room temperature, and annealing is required to move them. Single substitutional nitrogen produces strain in the diamond lattice, it therefore efficiently captures moving vacancies, producing the NV centers.[6]

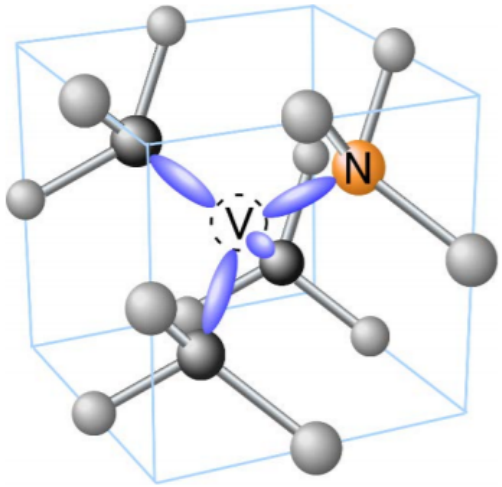

Figure 7: Representation of NV center in the diamond lattice. Vacancy is depicted as a circle in the middle of the diamond cage (gray balls are carbon atoms)[6].

Due to the symmetry of the diamond structure, there are four possible orientations of the NV center depending on the position of the nitrogen atom to the vacancy. Due to the lack of a carbon atom, there are four free bonds, one on each nitrogen atom and the three carbon atoms. In Figure 8 the orbitals of the free ties are shown. The NV center with the vacancy as the

origin can be assigned to the C_{3v} point group.

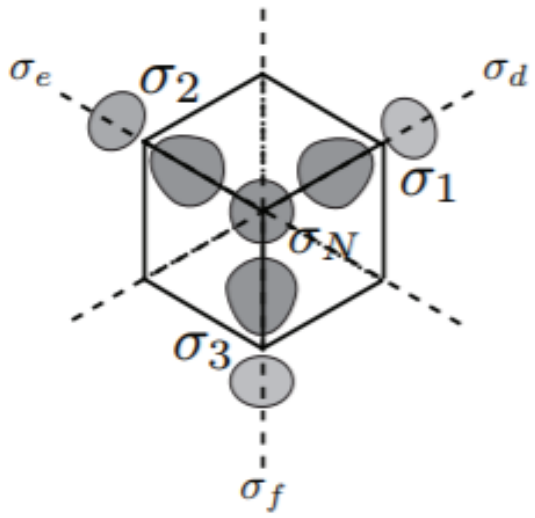

Figure 8: Schematic diagram of the dangling bond orbitals used to represent the NV defect.[7]

The centre is known to exist in negative (NV^-) and neutral (NV^0) charge states. The identifying features of NV^- and NV^0 are their optical zero phonon lines at 1.945 eV (637 nm) and 2.156 eV (575 nm), respectively, and associated vibronic bands that extend from their ZPLs to higher/ lower energy in absorption/emission. The sharp ZPLs and well defined vibronic bands of NV^- and NV^0 indicate that the optical transitions occur between discrete defect levels that are deep within the diamond bandgap, such that the continua of valence or conduction band levels are not involved in the optical transitions. An energy-level diagram of the NV center is shown in Figure 9. The basic photophysics can be explained by three electronic levels, including a ground state $|g\rangle$ of symmetry $^3A^2$, an excited state $|e\rangle$ of symmetry ^3E, and a metastable singlet state $|s\rangle$ that involves two levels with symmetries $^1A^1$ and ^1E. The ground and excited states are spin triplet ($S = 1$) and are further split into three spin sublevels. The main $|g\rangle \leftrightarrow |e\rangle$ transition has a resonant wavelength of 638 nm (zero phonon line) and can be efficiently excited at most wavelengths below 640 nm. Only a few percent of the photons are emitted into the zero phonon line, and most luminescence appears in vibrational side bands between 630 and 800 nm.

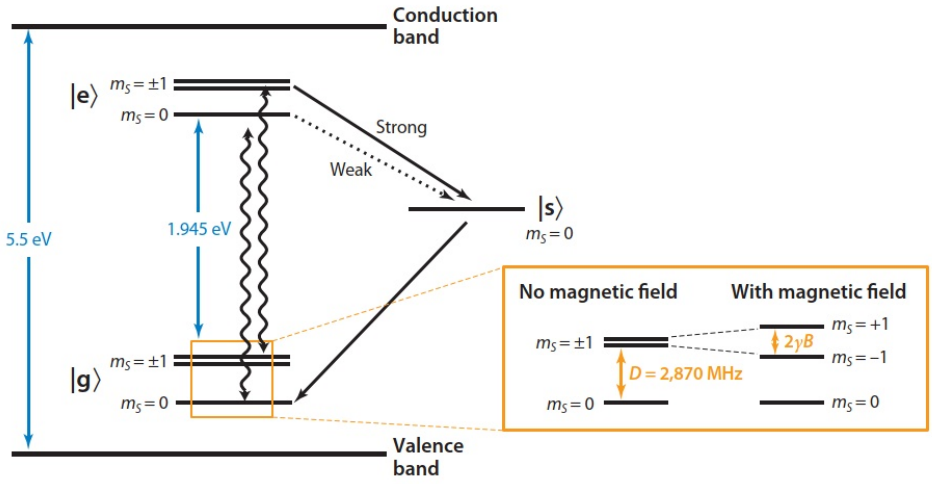

Figure 9: Energy-level diagram of (NV^-). $|g\rangle$ denotes the electronic ground state, $|e\rangle$ the electronic excited state, and $|s\rangle$ the metastable singlet state. Wiggly arrows indicate the radiative transition, and black arrows indicate strong and weak nonradiative decay via the singlet state. (Inset) The three spin sublevels with $m_S = 0$ and $m_S \pm 1$ at zero and nonzero magnetic field B. D is the zero-field splitting and $2\gamma B$ is the Zeeman splitting, where γ is the electron gyromagnetic ratio. By convention, the lower energy transition is associated with $m_S = -1$. [8]

NV centers emit bright red light ($^3E \rightarrow {}^3A$ transitions), if excited off-resonantly by visible green light ($^3A \rightarrow {}^3E$ transitions). This can be done with convenient light sources such as argon or krypton lasers, dye lasers, or He-Ne lasers. Excitation can also be achieved at energies below that of zero phonon emission.

As the relaxation time from the excited state is small ($\sim$ 10 ns), the emission happens almost instantly after the excitation. At room temperature the NV center's optical spectrum exhibits relatively sharp peaks, strongly overlaped by the thermally actived phonon sidebands.

2.1.6 Germanium Vacancy Centers

The germanium-vacancy center (GeV) is an optically active defect in diamond, which can be created by doping germanium into diamond during its growth or by implanting germanium ions into diamond after its growth. GeV

can behave as a single-photon source and shows potential for quantum and nanoscience applications due to its narrow zero-phonon line (ZPL) and minimal phononic-sideband (compared to that of the nitrogen-vacancy center (NV)).

The GeV center in diamond is formed when two adjacent diamond lattice carbons are replaced with lattice vacancies and an interstitial germanium atom, forming a split vacancy color center (Fig. 10). The resulting geometry is aligned along a $\langle 111 \rangle$ axis and has inversion-symmetric D_{3d} symmetry. This structure is identical to the SiV center in diamond [22] and leads to ${}^2E_g$ and ${}^2E_u$ ground and excited states, respectively. These have twofold degeneracy in both spin and orbit, which is partially lifted by spin-orbit interactions to produce levels labeled $1, 2$ (ground) and $3, 4$ (excited) in order of increasing energy. Transitions between these lead to a four-line fine structure of the zero-phonon line (ZPL), as shown in Figure 10. The $1 - 3$ transition possesses the highest photoluminescence (PL) amplitude, appearing as a single peak around 602 nm at room temperature accompanied by a weak phonon sideband containing about 40% of the fluorescence.

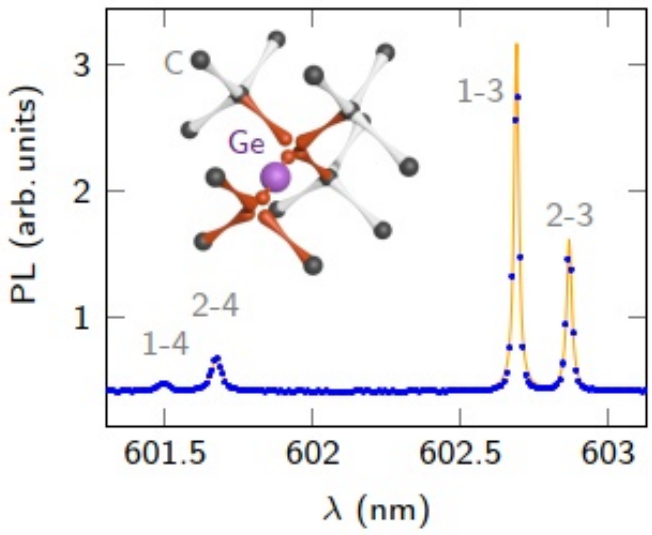

Figure 10: Crystal structure of the GeV color center in diamond and level structure and PL spectrum of GeV center.[9]

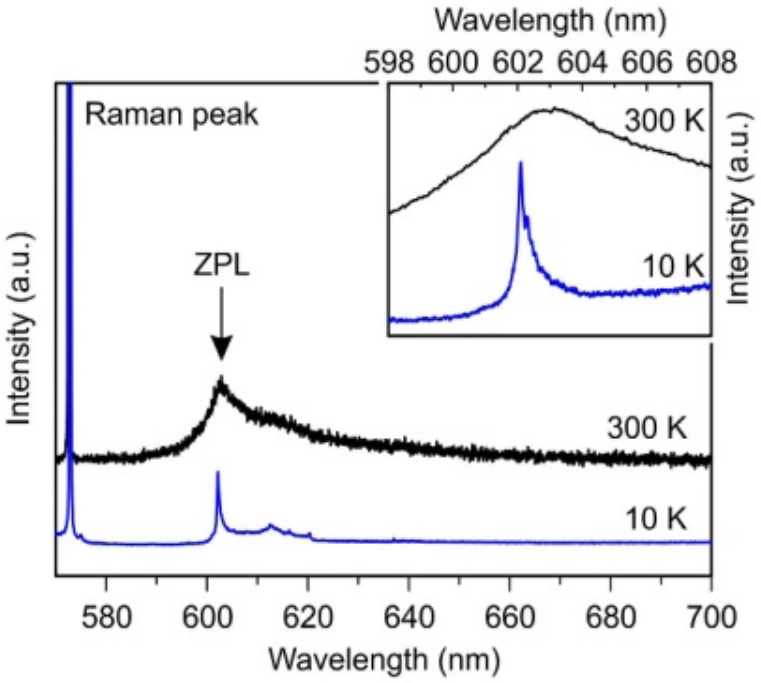

Figure 11: Experimental literature results of PL spectra from a Ge ion implanted diamond at 300 K and 10 K. The inset shows ZPL at both temperatures.[10]

2.1.7 Magnesium Vacancy Centers

Magnesium is a chemical element with the symbol Mg and atomic number 12. It is a shiny gray solid which bears a close physical resemblance to the other five elements in the second column (alkaline earth metals) of the periodic table: all group 2 elements have the same electron configuration in the outer electron shell and a similar crystal structure.

Magnesium is the ninth most abundant element in the universe. It is produced in large, aging stars from the sequential addition of three helium nuclei to a carbon nucleus. When such stars explode as supernovas, much of the magnesium is expelled into the interstellar medium where it may recycle into new star systems. Magnesium is the eighth most abundant element in the Earth's crust and the fourth most common element in the Earth (after iron, oxygen and silicon), making up 13% of the planet's mass and a large fraction of the planet's mantle. [11]

Magnesium related centers have only recently been discovered as new color centers. They are believed to involve vacancies (because single centres exhibit a strong polarisation anisotropy in excitation [12]). The fluorescence measured from the implantation spots shows the characteristic emission at 557.4 nm. The corresponding charge state is still unknown. No theoretical works have been done so far such that one could perfectly understand its structure inside the diamond. In this work, the same sample was used for investigation as in [12], due to the fact that Magnesium is extremely difficult to implant.

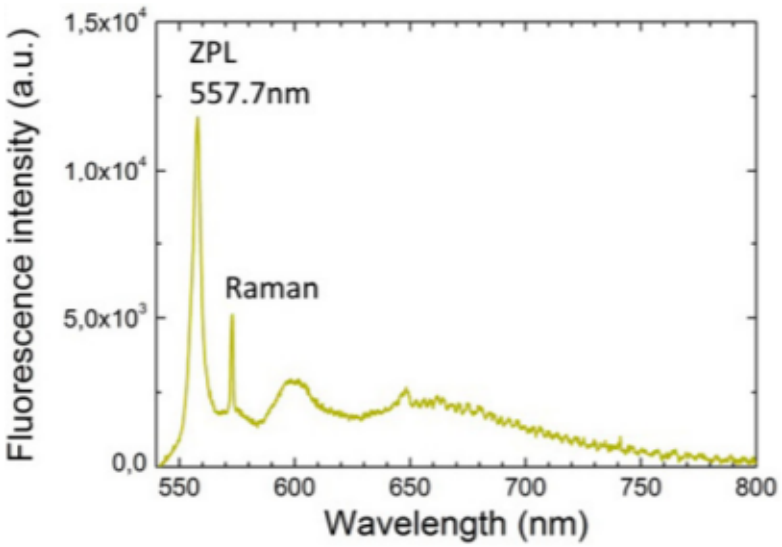

Figure 12: Experimental literature results of confocal fluorescence scan of Mg-related centres. [12]

2.2 Thermometry

Temperature is a physical quantity that expresses hot and cold. It is the manifestation of thermal energy, present in all matter, which is the source of the occurrence of heat, a flow of energy, when a body is in contact with another that is colder. Many physical processes are related to temperature, such as the physical properties of materials including the phase (solid, liquid, gaseous or plasma), density, solubility, vapor pressure, electrical conductivity, the rate and extent to which chemical reactions occur, the amount and

properties of thermal radiation emitted from the surface of an object, and the speed of sound which is a function of the square root of the absolute temperature. [13]

The Celsius scale (°C) is used for common temperature measurements in most of the world. It is an empirical scale that was developed by a historical progress, which led to its zero point 0°C being defined by the freezing point of water, and additional degrees defined so that 100°C was the boiling point of water, both at sea-level atmospheric pressure. Because of the 100-degree interval, it was called a centigrade scale [14]. Since the standardization of the Kelvin in the International System of Units, it has subsequently been redefined in terms of the equivalent fixing points on the Kelvin scale, and so that a temperature increment of one degree Celsius is the same as an increment of one Kelvin, though they differ by an additive offset of approximately 273.15.

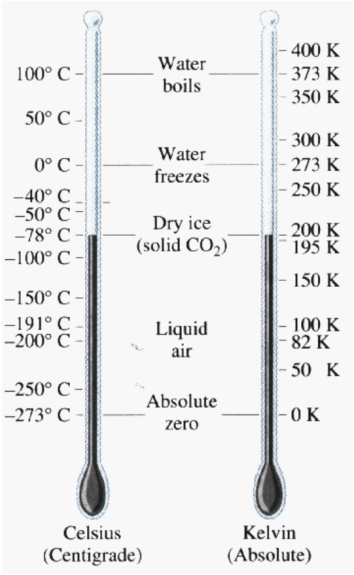

Figure 13: Temperature scale relation.[14]

Thermometry is the process of measuring temperature. Galileo Galilei's thermometer in 1603 utilized the expansion and contraction of air. However, as the air was sealed with the water which was exposed to the outside air, the height of the water surface, which indicates the temperature, was affected by the atmospheric pressure. Later, a thermometer was developed that con-

tained liquid in a tube, and it enabled temperature changes to be observed without being affected by atmospheric pressure. When the accuracy of the thermometer was improved in this way, there was also a person who tried to measure quantitatively with regular graduations on the tube. In 1701, Isaac Newton proposed that the liquid level of the thermometer set to zero, when the thermometer is inserted into melted ice, and that the temperature of the human body set to twelve, and divided that temperature difference by twelve. At that time, the thermometer used the expansion and contraction of water and alcohol, and the measurement range and accuracy were quite limited.

In the modern days, when measuring the temperature in our day-to-day life, but also when talking about macro-scale thermometers, we can differentiate between a couple of types of them. **Liquid in glass thermometer** is the oldest and widest type of temperature measurement device used nowadays. The main principle used is that of the apparent thermal expansion of the liquid used. It is the difference between the volumetric reversible thermal expansion of the liquid and its glass container that makes it possible to measure temperature. **Thermocouples** produce a voltage when one spot has a different temperature from the set reference temperature at another spot, this is done by use of two non-similar conductors. One of the many devices, that measure temperature, this one is unique for its use of stable, ductile-able platinum wire, it is called a **platinum resistance thermometer(resistance temperature detectors)**. Accurate readings are given when the wire used is pure, as it gives a constant proportionality between change in temperature and change in resistivity. Therefore, when current passes from the wire, we can get the voltage off a voltmeter, then calculate resistance. Now we can make use of the graph or derive an equation of calibration, to determine the temperature.

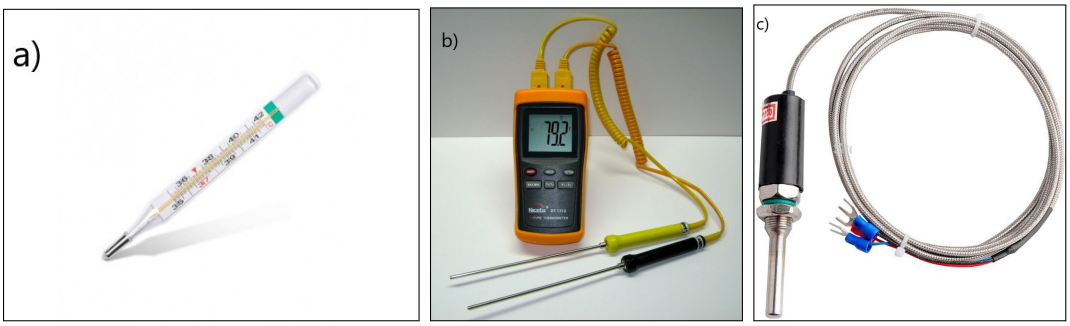

Figure 14: Examples of thermometers. a) Liquid in glass, b) Thermocouple, c) PT 100. [15]

Temperature sensing with spatial resolution is needed to improve stability, micro-fluidic devices, medical diagnostics and treatment. To be more specific, understanding the thermal properties of a living organism is a long-standing problem, since temperature is the most fundamental factor regulating all chemical reactions in vivo. Living cells actively react to environmental changes in temperature and are likely to change their internal temperature during such processes as division, gene expression, enzyme reaction, and metabolism. Therefore, real time monitoring of the thermal properties of cells and/or specific organelles opens the door to new possibilities for understanding intracell chemistry. Recently, high-resolution temperature measurement techniques made it possible to probe temperature fluctuations at the single-cell level and even within the cell. A number of different techniques for intracellular temperature mapping have been suggested in recent years. For example, fluorescent nanogel was used in combination with time-resolved photon counting, enabling temperature sensitivity of better than 0.5°C inside the cell. Local measurements with an ultrathin thermocouple were demonstrated to have a similar level of sensitivity. Another interesting technique is based on quantum dots and the dependence of their photoluminescence spectra on temperature. Probably the most precise measurement of temperature inside the cell was achieved using nitrogen-vacancy (NV) color center in diamond. Here, by controllably heating a cell via laser illumination of a gold nanoparticle, researchers were able to achieve the temperature resolution well below 0.1°C [16]. In addition to providing superior sensitivity, this method has a number of advantages related to the intrinsic properties of diamond: it is chemically and physically inert, is not porous and has low toxicity, and thus is expected to have a minimal effect on the cell (or organelle) func-

tionality. While an NV-center-based sensor provides the best temperature sensitivity, it has a considerable limitation due to the fact that it requires the application of microwave radiation to the diamond. Since microwave radiation cannot be focused below a cell's size, the cell must be exposed to its large dose. At the same time, microwave radiation can produce heating or otherwise influence cell chemistry. A possible alternative for the NV center may be a magnesium-vacancy (MgV) center or germanium-vacancy (GeV) center, which has optical spectra dominated by a zero-phonon line, thus, offering a possibility to measure temperature through detection of changes in the optical spectrum.

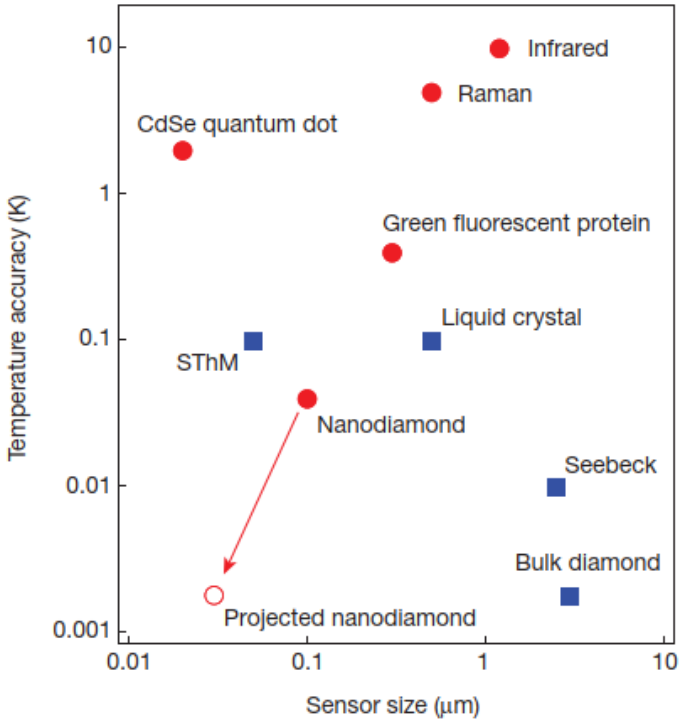

Figure 15: Comparison of sensor sizes and temperature accuracies for the nitrogen-vacancy quantum thermometer and other reported techniques. Red circles indicate methods that are biologically compatible. [16]

2.2.1 Nitrogen Vacancy Centers as Temperature Sensors

Diamonds imbedded with NV-centers have attracted much interest in recent years and have became a hot topic in many areas of research due to their unique properties such as magneto-sensitivity, photostability, and chemical inertia, which make the material a promising candidate for various applications in nanotechnology. Not much is known about temperature dependence of NV-emission above room temperature. Narrowing of the zero-phonon line, minor changes to the phonon-band structure, and most interestingly increase of the luminescence intensity at higher temperatures were reported below 200 K. Sensitivity of NV-embedding diamonds to surrounding temperatures could complement their already known characteristics and would form a basis for using these crystals also for temperature-mapping with nanometer spatial-accuracy.

In the applications of NV^- electron spin, one of the most concerned is the transition between sublevels of the ground state, which can be well studied by the optically detected magnetic resonance (ODMR) method. In Chen *et.al* [17], a series of ODMR spectra (Fig.16) for the sample at temperatures ranging from 5.6 K to 295 K was measured. The zero field splitting parameter D nonlinearly depends on temperature and is getting larger with temperature decreasing. The change is $\Delta D \approx 7$ MHz between 5.6 K and 295 K.

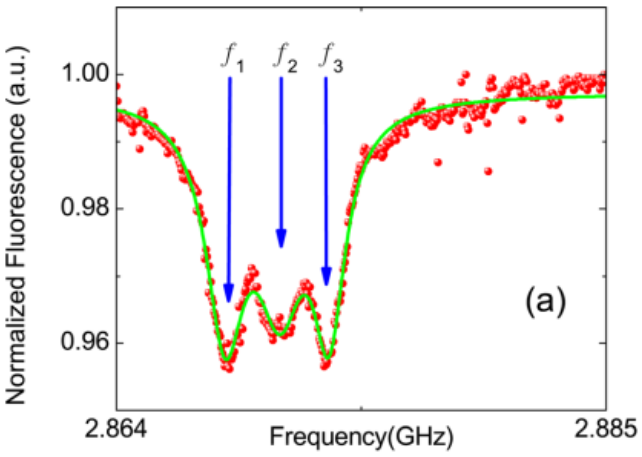

Figure 16: ODMR spectrum of NV^- ensemble at 294 K. The three peaks are indicated by arrows, and the green solid line represents the fit of Lorentz function [17].

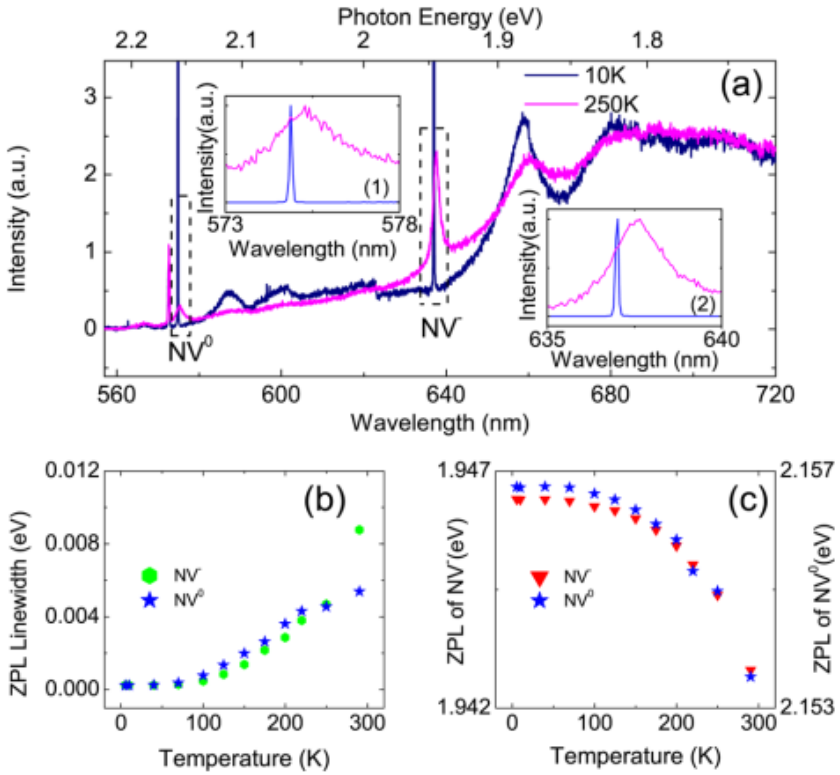

Figure 17: a) Fluorescence spectra at 250 K (red line) and 10 K (blue line). The insets (1) and (2) show the normalized ZPL details of NV^0 and NV^-, respectively. The changes of linewidth (b) and photon energy (c) are obtained in the spectra [17].

The literature results indicate that the temperature dependent shifts are universal for different charge states and different energy gaps. All the shifts should have the same origin, which is the intrinsic property of this defect. An important conclusion is made in [17], more specifically, that the local atomic structure should be taken into consideration for the shifts, meaning that the local expansion, rather than bulk's, is the one responsible for the energy shift.

2.2.2 Germanium Vacancy Centers as Temperature Sensors

The idea of GeV-based thermometry is based on optical measurements of the spectral shift of the zero-phonon line and its spectral width with the tem-

perature changes. The rate of electron−phonon interaction is much higher than the spontaneous decay rate of the exited state in a wide range of temperatures, leading to the strong temperature-dependent modification of the line width of transition and a shift of its position. In previous literature works on this topic, the temperature-dependent changes in the PL signal were were analyzed by fitting the fluorescence spectrum of the GeV ZPL and phonon sideband with different Lorentzian functions depending on the PL signal-to-noise ratio for that measurement [18]. A single Lorentzian function ($L1$) provides a stable fit for noisier data taken at lower laser powers, while double Lorentzian function ($L2$) provides a stable fit with much less error in the center (λ_c) and full width half maximum (fwhm) (λ_W) wavelength fit parameters for higher laser powers (Fig. 18).

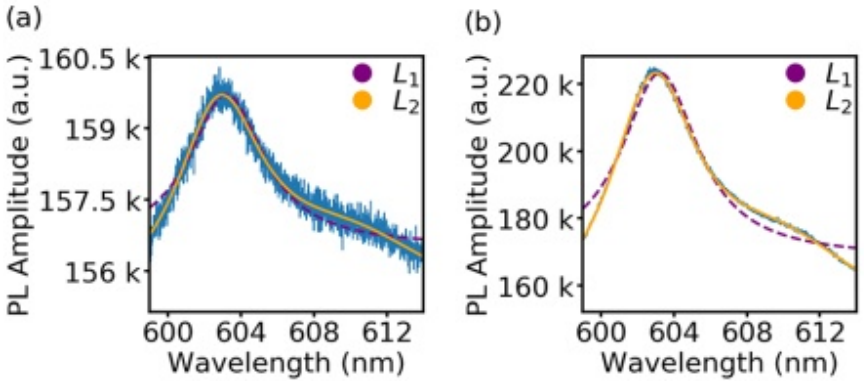

Figure 18: Literature experimental results. Single and double Lorentzian fit functions (purple, orange traces) for spectra collected with laser powers of (a) 1 mW and (b) 20 mW at 500 ms exposure time. [18]

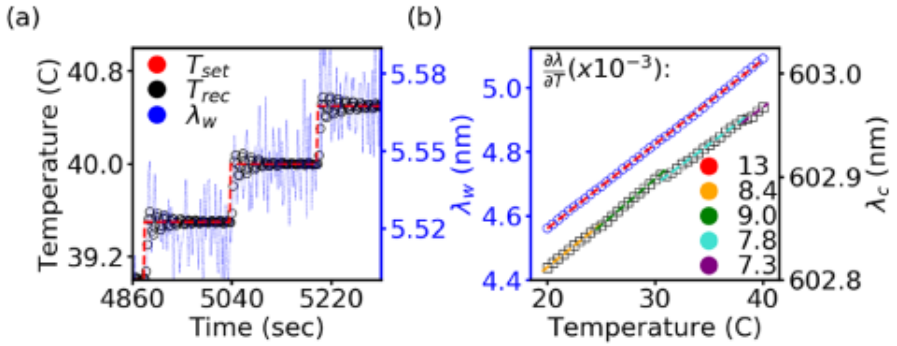

Figure 19: Literature experimental results. a) Plot of measured temperature versus time for a step dwell time of 3 min. The thermal controller takes more than 2 min to fully settle. b) Plot of GeV fluorescence peak width (λ_W, blue circles) and center wavelength (λ_C, black squares) versus temperature. [18]

2.3 Energy Level Shift of Color Centers Described by Modified Varshni Model

In the conventional semiconductor materials, it is generally accepted that the temperature dependent energy gap shift is due to the electron-(acoustic and optical) phonon interaction effect and thermal expansion effect. This is a very complicated process, although in experiments the energy gap shift usually exhibits some simple monotonic behavior as a function of temperature T. For the study of NV color centers in previous literature, a fifth-order polynomial function has been proposed to fit the experimental data of for temperature lower than 300 K. While at high temperature ranging from 300 K to 700 K,the data can be well described by a third-order polynomial function.

In experiments the much referenced Varshni empirical equation [42]:

$$E(T) = E_0 - \frac{\alpha T^2}{T + \beta} \tag{7}$$

has been used to describe the temperature dependent energy gaps in various conventional semiconductors. The parameters α and β are positive to ensure the monotonicity of energy gap as a function of temperature. The value of β is generally believed to be related and comparable to the Debye temperature Θ_D. This empirical equation has turned out to be an extreme

success in the history of fitting the temperature dependent energy gaps in many semiconductor materials.

Unfortunately, the Varshni empirical equation fails to describe the energy gap shifts in diamond. Although the diamond has the similar atomistic structure (diamond cubic) and symmetry as many other semiconductor materials, it still possesses some unique features, which are not shared by other semiconductors. For instance, the Debye temperature ($\Theta_D = 2200$ K) and optical phonon frequency ($\omega \sim 165.2$ meV) are generally $3-4$ times larger than those in other conventional semiconductor materials such as Si (diamond cubic structure) and GaAs (Zinc-blende structure). Moreover the lattice expansion coefficient in diamond is much smaller than those in other semiconductors. Therefore, at low temperature, this energy gap shift should be more accurately described by the Debye model, in which the electron phonon matrix is linearly proportional to the momentum $k = |k|$. This gives the well-known scaling law, $E(T) - E_0 \propto T^4$, which has been found in semiconductor Si at extremely low temperature. However, this assumption is insufficient when considering the real condition that the electron-phonon coupling strength should decay to zero very fast for large momentum k. In the simplest case when the coupling strength can be written as $k/(1 + Bk^2)$, where B is a positive constant, the energy gap should decay as T^2 in the high temperature regime (yet still much smaller than the Debye temperature Θ_D). Therefore, for NV^- centers in diamond, the above two interesting limits can be interpolated by the following modified Varshni formula [19],

$$E(T) = E_0 - \frac{AT^4}{(T+B)^2} \tag{8}$$

The two parameters A and B are restricted to positive values.

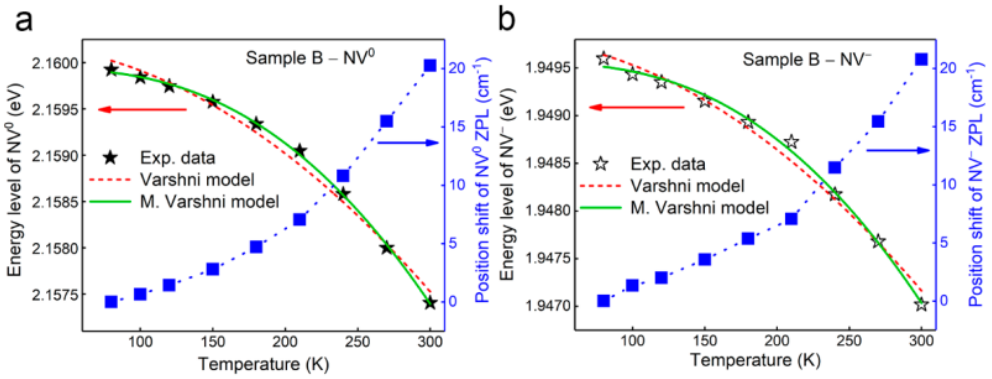

Figure 20: The ZPL position and energy level variation of (a) NV^0 and (b) NV^- centers with temperature including the proposed Varshni model fit.[21]

Finally, one should point out that the modified Varshni formula can also be applied to study the other type defects in diamond, as shown in the Table 1. [19].

Parameters	NV^0	SiV	NE8	NV^-
A ($\times 10^{-7}$ eV/K^2)	2.2(10)	2.3(7)	6.3(21)	0.5(1)
B(K)	418(157)	419(155)	579(140)	608(168)

Table 1: Parameters of modified Varshni equation fitting for the temperature dependent ZPL shifts of different defects in diamond [19].

3 Experimental Procedure

3.1 Linear Accelerator

Elements required to create the colour centers inside the diamond were implanted using the linear accelerator. Accelerator used has a maximum acceleration voltage, $U_{max} = 100$ kV and uses a Cesium sputtering source (Source of Negative Ions by Cesium Sputtering, SNICS II for short). In the source positively charged cesium ions are applied to a target made of the implantation material accelerated. The particles knocked out can, if they are not already, get negatively charged by the Cesium and move through the extractor to the acceleration section. Between the source and the end of the acceleration path, the desired acceleration voltage U is set. Then the negatively charged ions move through a 90° magnets. This acts as a mass filter by using the Lorentz force and various apertures. The magnetic flux density B_{mag} in the 90°-magnet is approximately proportional to the flowing current I_{mag} as long as the iron core of the magnet does not show any saturation effects. The proportionality factor results from the maximum current $I_{max} = 152$ A and the resulting magnetic flux density $B_{max} = 1.05$ T. The filtered masses m (I_{mag}) result from the condition of a stable trajectory of the ions (charge q) with a magnet's radius of curvature $r = 0.5$ m:

$$m(I_{mag}) = \frac{I_{mag}^2 r^2 B_{mag}^2 q}{2U I_{max}^2} \tag{9}$$

The particle flow can be measured with the aid of a Faraday cup[2] behind the sample. The structure of the accelerator is shown in Figure 21.

[2] A Faraday cup is a metal (conductive) cup designed to catch charged particles in vacuum. The resulting current can be measured and used to determine the number of ions or electrons hitting the cup. The Faraday cup was named after Michael Faraday who first theorized ions around 1830.

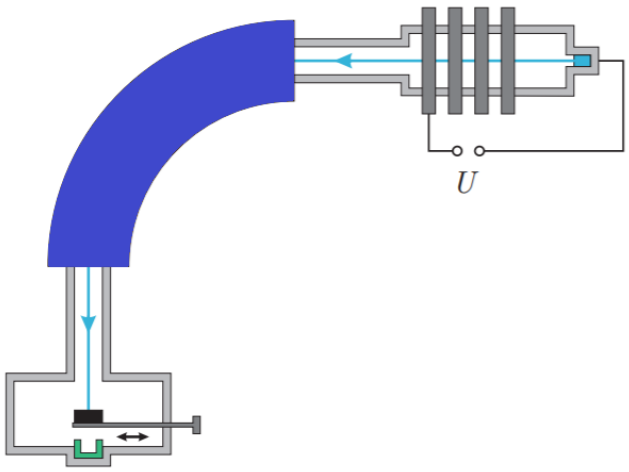

Figure 21: Sketch of the linear accelerator.

The diamond, ⟨100⟩, used in this thesis has been implanted with Nitrogen and Germanium with different energies and doses. Magnesium was investigated from a separate diamond sample, used in work by Lühmann *et.al* [12]. Sketch and image of the sample is shown in Figure 22.

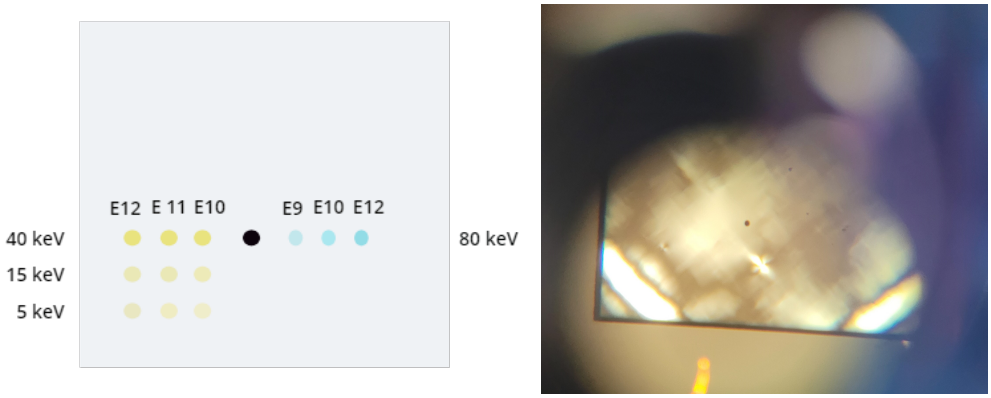

Figure 22: Sketch of the diamond implanted with Nitrogen (in yellow) and Germanium (in blue) with respective doses and energies of implantation. The black spot in the middle represents a graphite spot used for orientation purposes. Shown is also an image of the sample through optical microscope with the graphite spot visible.

3.2 Oven

To generate color centers, it is necessary to heat the diamond in a furnace after implantation. The duration of the heating process plays a role and temperature plays an important role. The HTR1001 heating element used here comes from Company Tectra and is located in a vacuum chamber.

The sample is placed on the Boralectric heating element with a heat shield covered and the oven closed. With the help of a mechanical and turbo vacuum pump, a vacuum in the range of 10^{-5} to 10^{-6} mbar is generated. Subsequently the heating power is set via an external current/voltage regulator. The temperature is measured just below the heating plate with a tectra HC3500 heating controller.

In order to generate NV and MgV centers, temperature of 800° C was used and the sample was annealed for 4 hours. For generation of GeV centers, temperature of 1200° C was used and the annealing lasted 4 hours.

3.3 Oxygen Plasma Etching

A plasma system from Diener electronic was used to clean diamond surfaces. After the sample is removed from the oven, a visible film on the top of the sample is formed, whose composition is a carbon based material. It is a consequence of the dissociation of air introduced in the oven chamber from the existent leakage. In order to remove it, we have used passive oxygen plasma etching. The sample is placed in an evacuated glass cylinder on a hot plate. The system can be operated at room temperature or at higher temperatures. Two electrodes, which are connected to a high-frequency generator, are arranged around the glass cylinder. The desired gas is fed into the cylinder and the generator generates a plasma by capacitive-electrical excitation. The cylinder of the system used has a volume of 5 l and the high-frequency generator delivers a frequency of 40 kHz. The maximum achievable power is 200 W.

3.4 Chemical Cleaning

In order to remove any type of rest contaminants (mainly metallic, for example introduced during the sample handling with the tweezers etc.), the samples have undergone chemical cleaning. All samples were cleaned by immersion in a mixture of 30 ml concentrated sulfuric acid (H_2SO_4), 10 ml of

concentrated nitric acid (HNO_3) and 10 ml of 60% perchloric acid ($HClo_4$). This mixture was heated ($T \approx 130°C$) for 4 hours under reflux. After cooling to room temperature, the acids were decanted and the diamonds were washed intensively with distilled water.

3.5 Confocal Microscope

The optical excitation and the detection of the fluorescence radiation takes place with an aid of a confocal microscope. A homemade scanning confocal fluorescence microscope was used, with an air objective. There is a pinhole in front of the detector, in this case a photodiode. Light can only pass through the aperture completely if the focus point lies in the diaphragm plane. This means that only light can come from a certain depth of the sample. There is light from other depths more or less blocked by the diaphragm and only contributes to a limited extent to the measurement (Fig. 23). Because of this structure, it is possible to target specific levels in certain depths without other levels contributing to the measurement. Laser excitation used was at 532 nm (green laser) and at 488 nm (blue laser). The laser reflection was suppressed by a suitable Notch filter and the collected signal has consequently been imaged onto a 0.2 nm resolution narrow band spectrometer. Power of both lasers was kept at ≈ 1 mW along with 1000 ms exposure time.

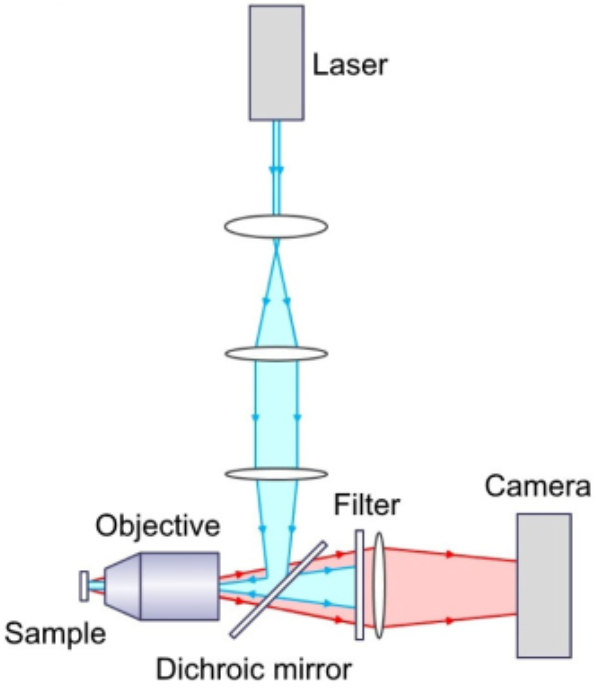

Figure 23: Sketch of the confocal microscope[12].

3.6 Temperature Controller

Temperature control is a process in which change of temperature of a space (and objects collectively there within), or of a substance, is measured or otherwise detected, and the passage of heat energy into or out of the space or substance is adjusted to achieve a desired temperature. A device used for such purpose is called the temperature controller. It's working principle is to first measure the temperature (process variable), it then compare it to the desired value (set value). The difference between these values is known as the error (deviation).

A home-made temperature controller was used in this works. It consists of a sample holder which is made out of copper and teflon (see Figure 24). Materials are chosen due to their physical properties. Copper has excellent heat conductivity, it is non magnetic, has melting point at 1083°C with thermal expansion of 17×10^{-6} strain/°C. Teflon has excellent thermal and

electrical insulation with thermal expansion coefficient of 1.7×10^{-4} strain/°C.

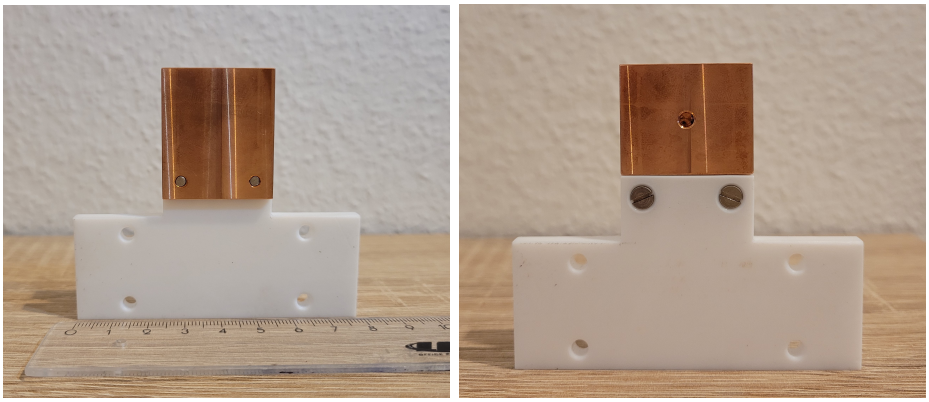

Figure 24: Image of the built sample holder, front and back side, respectively.

The sample holder has two holes in the copper block, one from above and one from behind. They host two small but crucial pieces of equipment, namely, a heating element and a PT100 which is a resistive temperature device that detects the temperature set by a temperature controller (all the pieces are produced by company ThorLabs) (Fig. 25). For controller to reach temperature stabilization, between 3 to 5 min are needed and the stability is better then 100 mK.

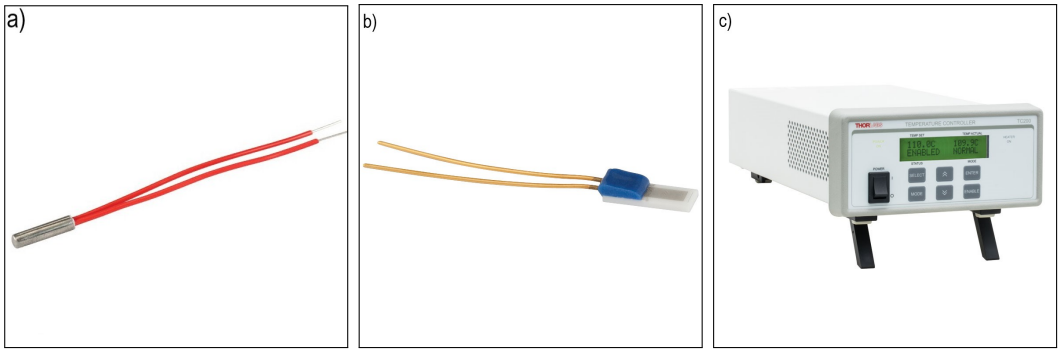

Figure 25: a) HT15W Miniature Cartridge Heating Element, b) THPT100 100 Ω Resistance Temperature Detector, c) TC200 Temperature Controller [20].

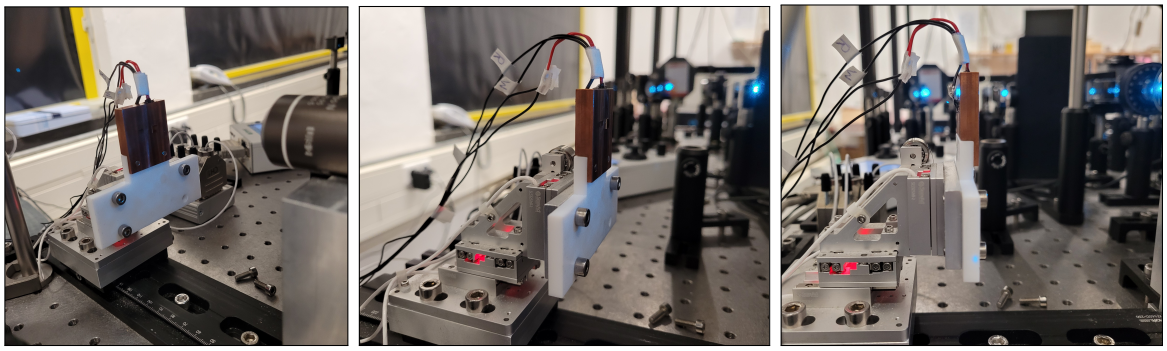

Figure 26: Images of the built sample holder integrated to the confocal microscope setup.

4 Experimental Results

4.1 Creation of Color Centers

In order to confirm the successful creation of color centers by method of implantation in the diamond, photoluminescence measurements were firstly performed at usual conditions (room temperature, without the use of the temperature controller) with the use of green laser.

4.1.1 Nitrogen Vacancy Centers

Nitrogen was implanted in the 4×4 mm, $\langle 111 \rangle$, diamond sample using 3 different implantation energies, namely, 40 keV, 15 keV and 5 keV and three different doses (ion fluence of 1×10^{10} cm^{-2}, 1×10^{11} cm^{-2} and 1×10^{12} cm^{-2}). The choice of ion kinetic energy ensures control of the penetration depth. SRIM calculations were done in order to determine the corresponding depths and results are presented in Figure 27.

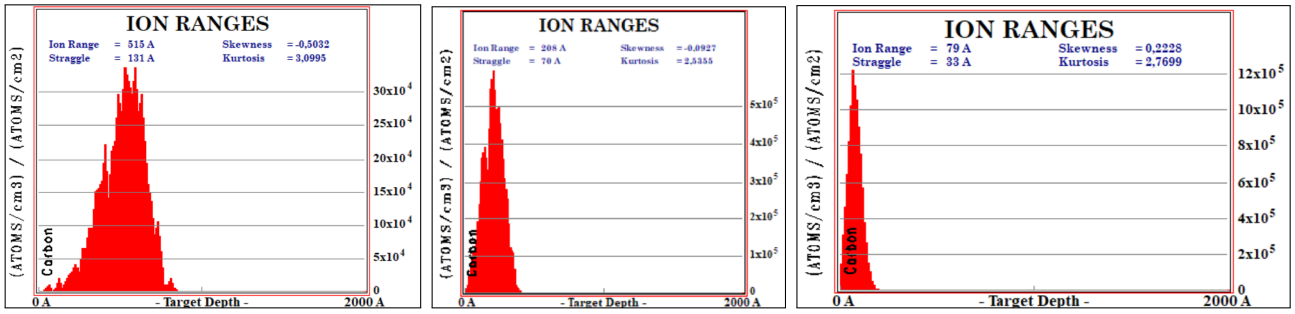

Figure 27: SRIM depth calculation of 40 keV, 15 keV and 5 keV, respectively.

From the simulations, it is visible that the corresponding penetration depths are 51.5 nm for 40 keV, 20.8 nm for 15 keV and 7.9 nm for 5 keV.

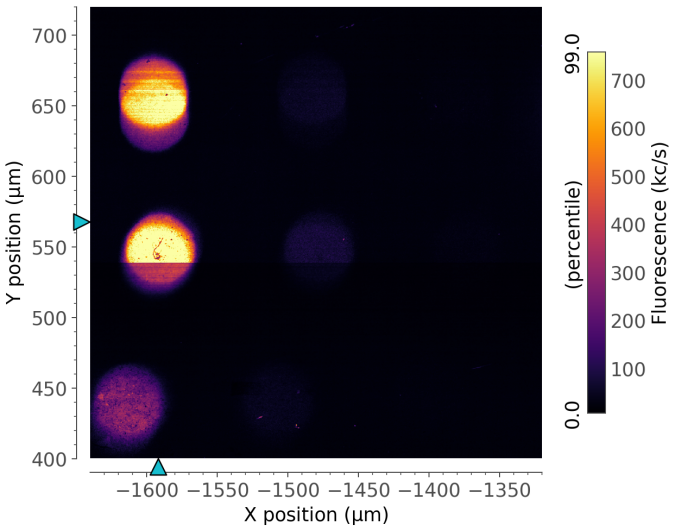

Figure 28: Optical image of the implanted NV centers.

Photoluminescence measurements indeed show presence of the NV^0 (at 575.2 nm) and NV^- (at 638.2 nm) centers as shown in figures 29, 30 and 31.

Position of the peaks in the PL spectra follow

$$E(eV) = \frac{1.24}{\lambda(\mu m)} \tag{10}$$

$$\Delta E = E_0 - E \tag{11}$$

$$S_R = \frac{10^4}{\Delta\lambda} \tag{12}$$

where $\lambda(\mu\text{m})$ is wavelength of the incident or emission photon, $E(\text{eV})$ is the corresponding energy of the photons, $S_R(\text{cm}^{-1})$ is the Raman shift, and $E_0(\text{eV})$ is about 2.33 eV, corresponding to the photon energy of 532 nm incident photon.

Fluorescence emission intensity of NV^0 and NV^- centers depend not only on the power of the excitation photons but also the concentration of NV centers in diamond. The decrease in the intensity indicates the decrease in NV center concentration in diamond, which can be attributed to the formation of other types of nitrogen vacancies in diamond, such as pairs or clusters,

instead of NV centers, leading to the decrease in NV center concentrations in diamond [21].

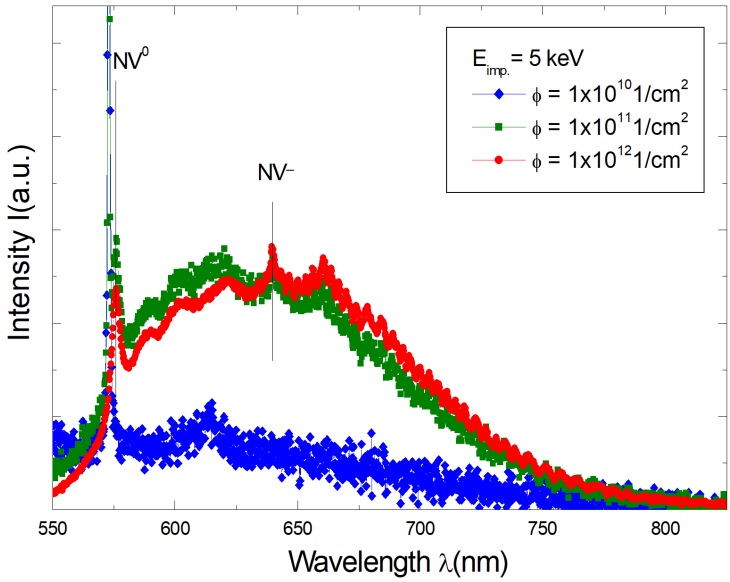

Figure 29: Photoluminescence spectrum measured at room temperature of part of the sample irradiated with implantation energy of 5 keV with the use of green laser.

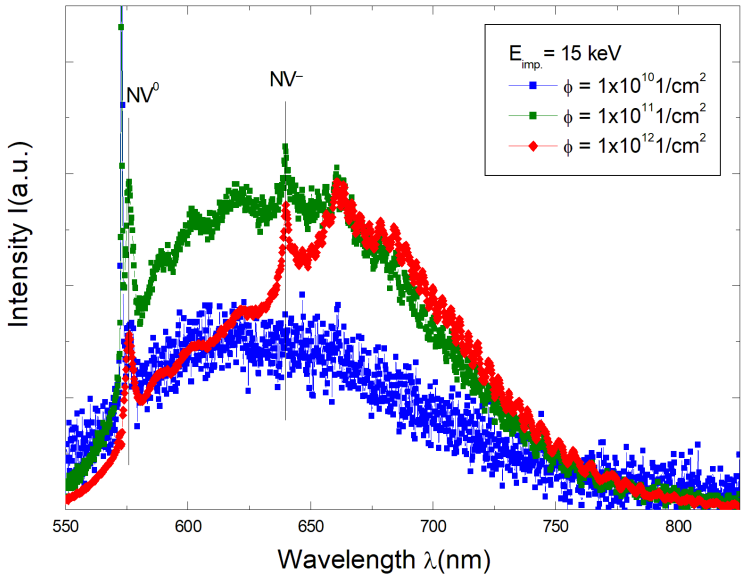

Figure 30: Photoluminescence spectrum measured at room temperature of part of the sample irradiated with implantation energy of 15 keV with the use of green laser.

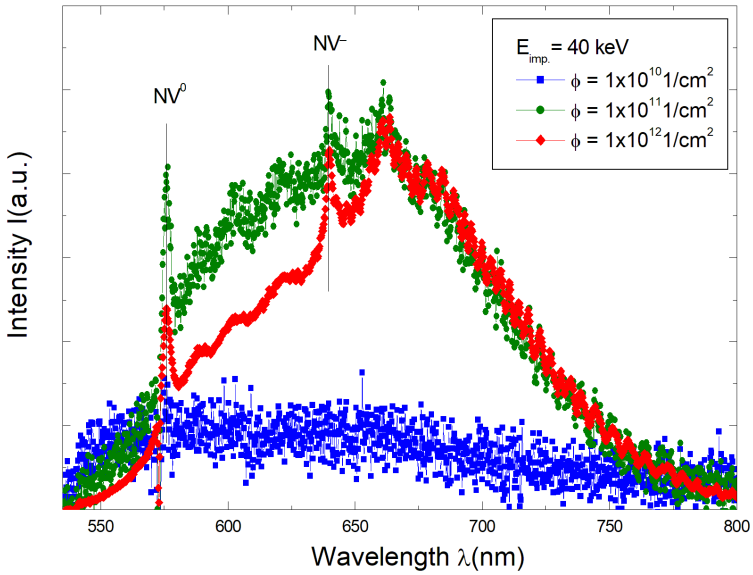

Figure 31: Photoluminescence spectrum measured at room temperature of part of the sample irradiated with implantation energy of 40 keV with the use of green laser.

4.1.2 Germanium Vacancy Centers

Germanium was implanted in the same 4×4 mm, $\langle 111 \rangle$ diamond sample, using one implantation energy, 80 keV and two different doses (ion fluence of 1×10^{10} cm^{-2} and 1×10^{12} cm^{-2}). As before, SRIM simulation was used in order to estimate the penetration depth, which in this case corresponds to 33.1 nm. Result of the simulation is shown in Figure 32.

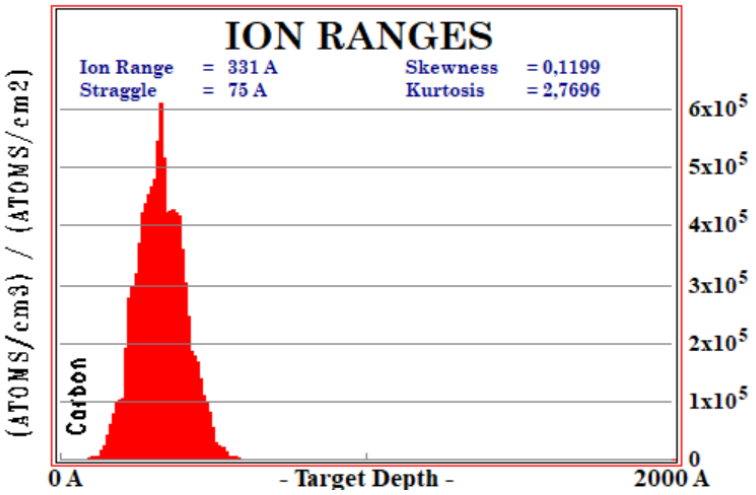

Figure 32: SRIM depth calculation for Germanium implantation.

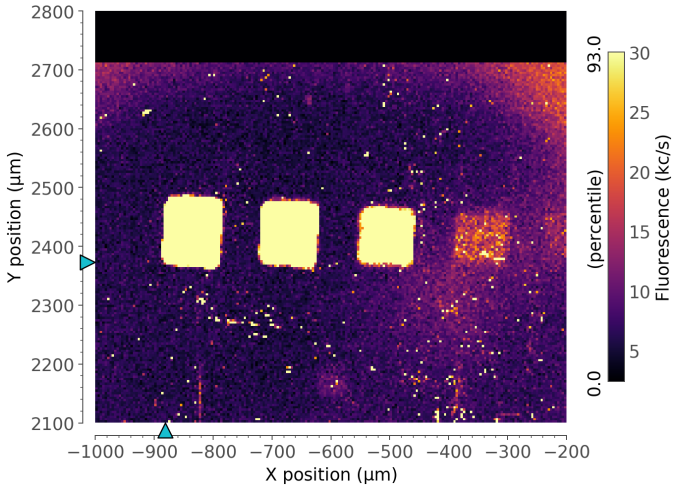

Figure 33: Optical image of the implanted GeV centers.

Photoluminisence measurements confirm the creation of GeV centers (Fig. 34). Both doses show a clear peak at 602.42 nm and a 200 nm broad phonon sideband, as experimentally confirmed in the literature [22]. Comparison of the results with the literature can be observed in Figure 35.

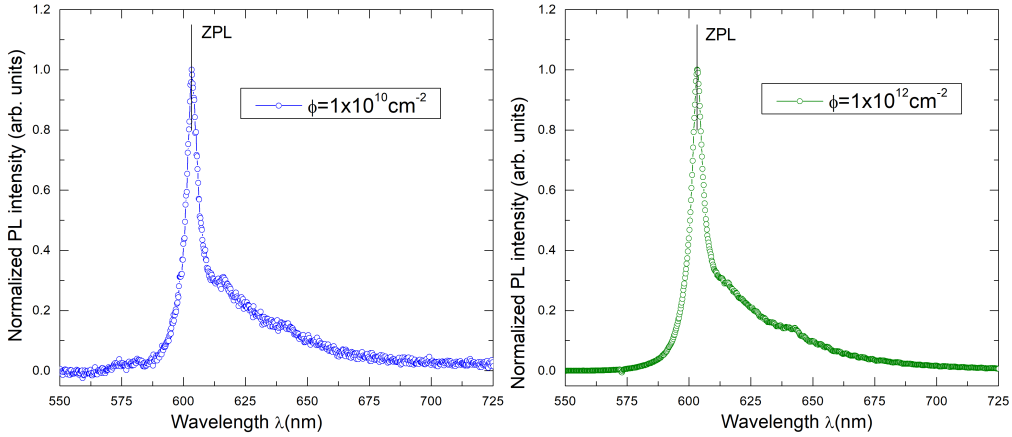

Figure 34: Photoluminiscence spectrum of GeV measured at room temperature with the two doses. Results were obtained with green laser.

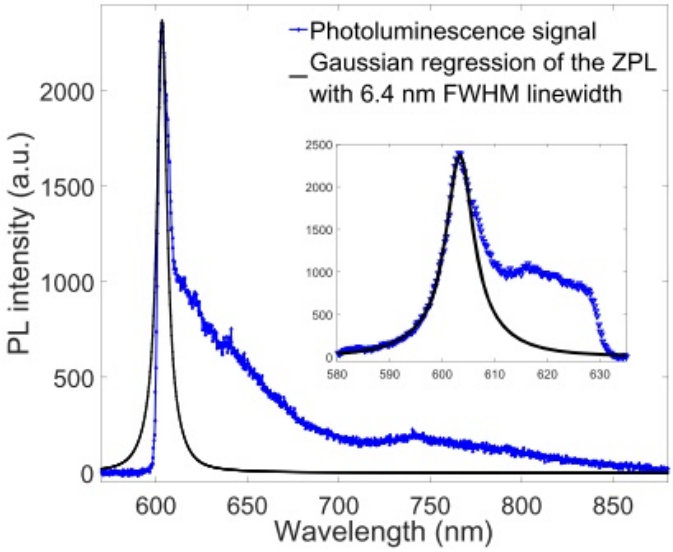

Figure 35: Literature results of PL spectrum of GeV ensamble. Blue line is the experimental result and the black the Gaussian regression of ZPL [22].

4.1.3 Magnesium Vacancy Centers

As mentioned before, MgV investigation took place on a different diamond sample (2×2 mm, $\langle 100 \rangle$) [12]. Magnesium was implanted with 50 keV

implantation energy (ion fluence of 1×10^{13} cm^{-2}), which corresponds to penetration depth of 49 nm. SRIM calculation is shown in Figure 36.

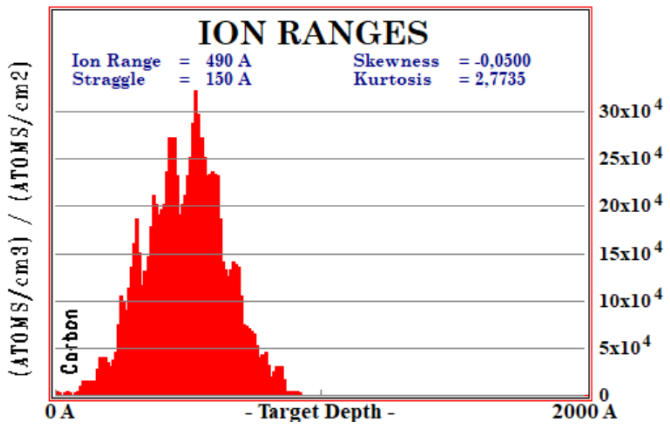

Figure 36: SRIM depth calculation for Magnesium implantation.

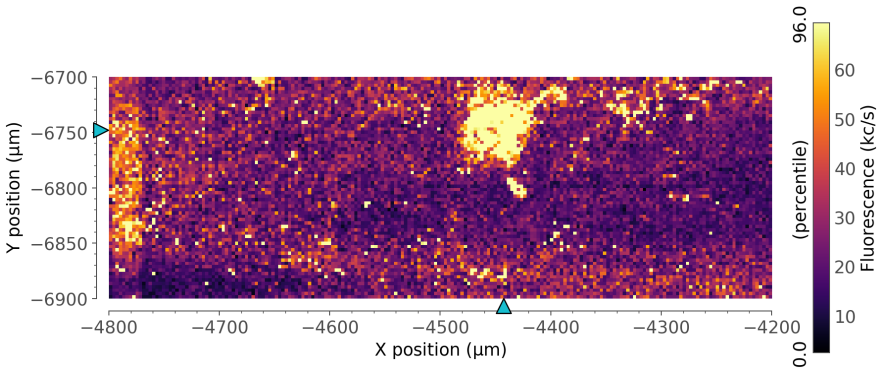

Figure 37: Optical image of the implanted MgV centers.

Creation of MgV centers was confirmed by PL measurement at room temperature (Fig. 38). Flourescence spectrum possesses a sharp and intense ZPL at 557.4 nm and the vibronic sidebands.

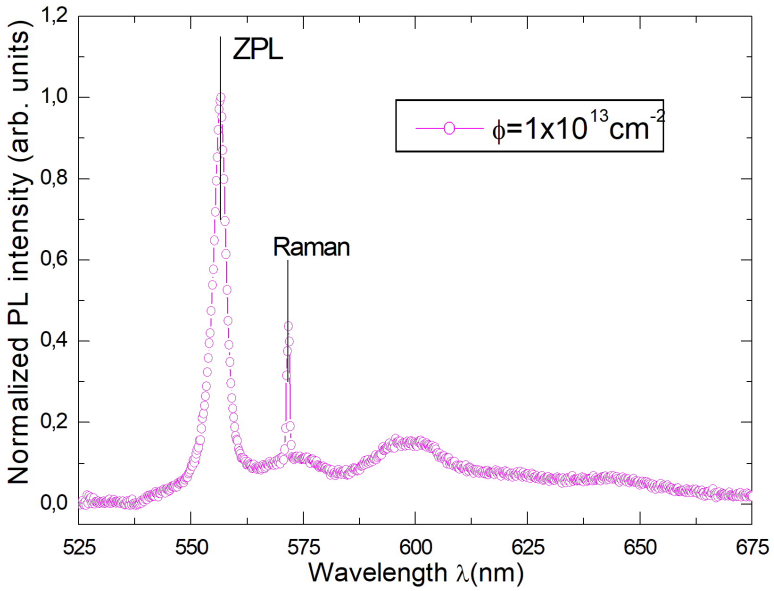

Figure 38: Photoluminescence spectrum of MgV measured at room temperature with green laser.

4.2 Temperature-Dependent Photoluminescence Measurements

In order to perform the temperature-dependence measurements, the built temperature controller with the new stage was used. Measurements were performed in the range between 20°C and 50°C. To be sure that the temperature stabilization is reached and the temperature gradient minimized, I have waited 10 min.

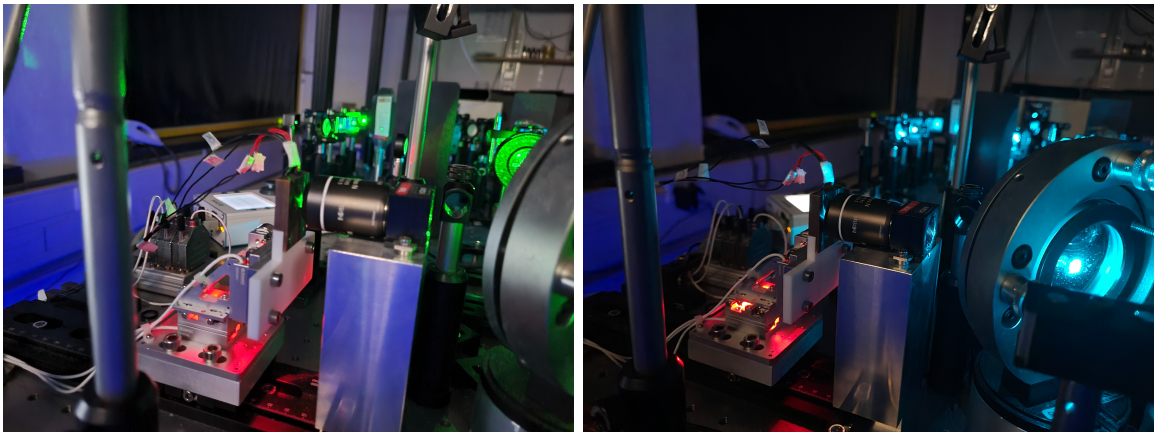

Figure 39: Images of the stage designed for temperature measurements illuminated with two lasers used.

4.2.1 Nitrogen Vacancy Centers

In the literature, NV centers as temperature sensors are very well described with the use of the green laser [36, 38]. For this and scientific curiosity reasons, in this work blue laser was used. Collected photoluminescence spectra together with the fits is shown in Figure 40. Fit was done using one Lorentzian function, and the attention is focused on the shifts of the NV^- and NV^0 peaks. The one Lorentzian function in this case makes sense because the complete spectrum is strongly dominated by the phonon sidebands, which is evident to see in Figure 40.

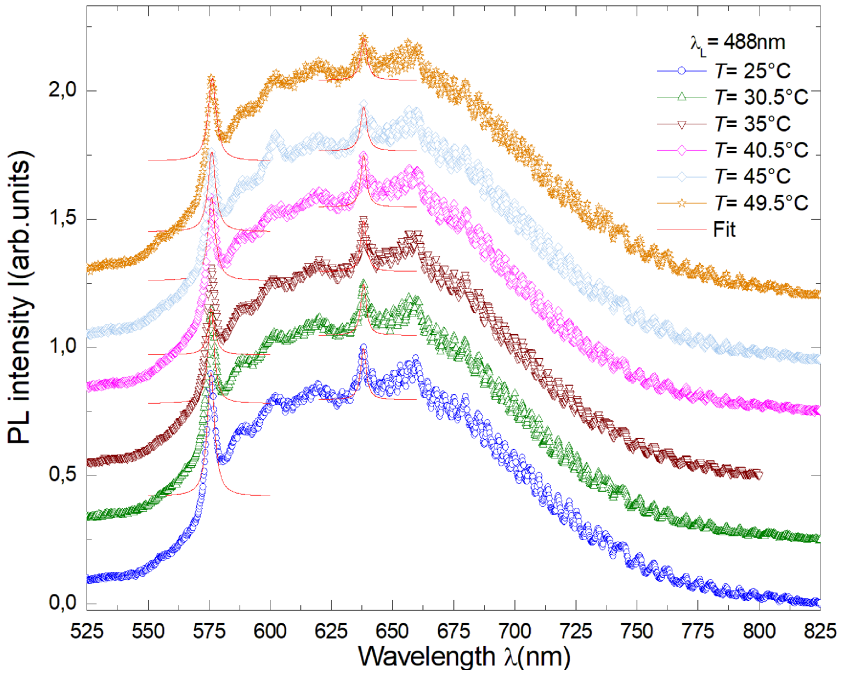

Figure 40: Photoluminescence spectrum of NV centers taken at 6 different temperatures with ≈ 5°C steps together with the Lorentz fits.

For analysis purposes, the wavelength related to the central peak of the Lorentz function which describes our ZPL or in this specific case of the NV^- peak, we call λ_C, and we keep this assumption in the rest of this work. The λ_C results obtained are plotted in Figure 41. As we already introduced and discussed in section 2.3, the changes of the ZPL with the temperature will be described under the modified Varshni theory.

The fit curve describing λ_C, according to Equation 8 possesses parameter $A = 4.083 \times 10^{-8} \pm 0.5258 \times 10^{-8}$ eV/K^2 (Fig. 41). Our results are in complete agreement with the literature (for comparison see Table 1.) [19]. Small difference comes from the fact that the literature results are investigated in a larger range of temperatures ($\approx$ 250 K), while we are focused on the investigation in the smaller range ($\approx$ 30 K).

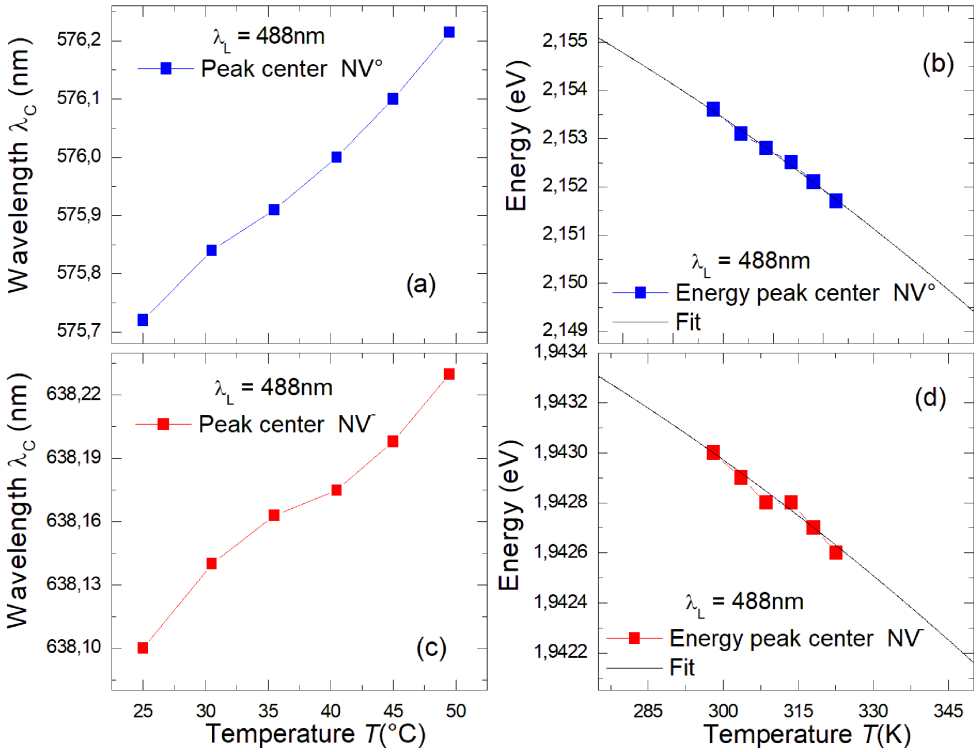

Figure 41: a) Plot of NV^- flourescence central wavelength (λ_c) vs temperature. (b) Plot of the energy $E(\lambda_c)$ central peak vs temperature, the line is the results of the fit done using the Equation 8. c) Plot of NV^- flourescence central wavelength (λ_c) vs temperature. (d) Plot of the energy $E(\lambda_c)$ central peak vs temperature, the line is the results of the fit done using the Equation 8.

4.2.2 Germanium Vacancy Centers

As in the case of NV centers, GeV centers as temperature sensors are well described in the literature by use of green laser [18]. In this work, the green laser was used in order to confirm previous results, and blue laser was used to investigate if there exist any difference or correlation with the wavelength.

Taking into account that the dose, in case of temperature measurements, doesn't play a role since results are the same, in this work in case of GeV centers only the dose of 1×10^{10} $1/\text{cm}^2$ was used.

Firstly, results obtained using the green laser are presented. Here, a clean

region of the sample was measured and used as background and subtracted from the measured PL spectra, therefore normalized to the maximum of the characteristic ZPL. Results can be seen in Figure 42, together with the fits that were done to each temperature measured. Three Lorentzian functions were used to fit the whole spectra, as they allow the most stable fit.

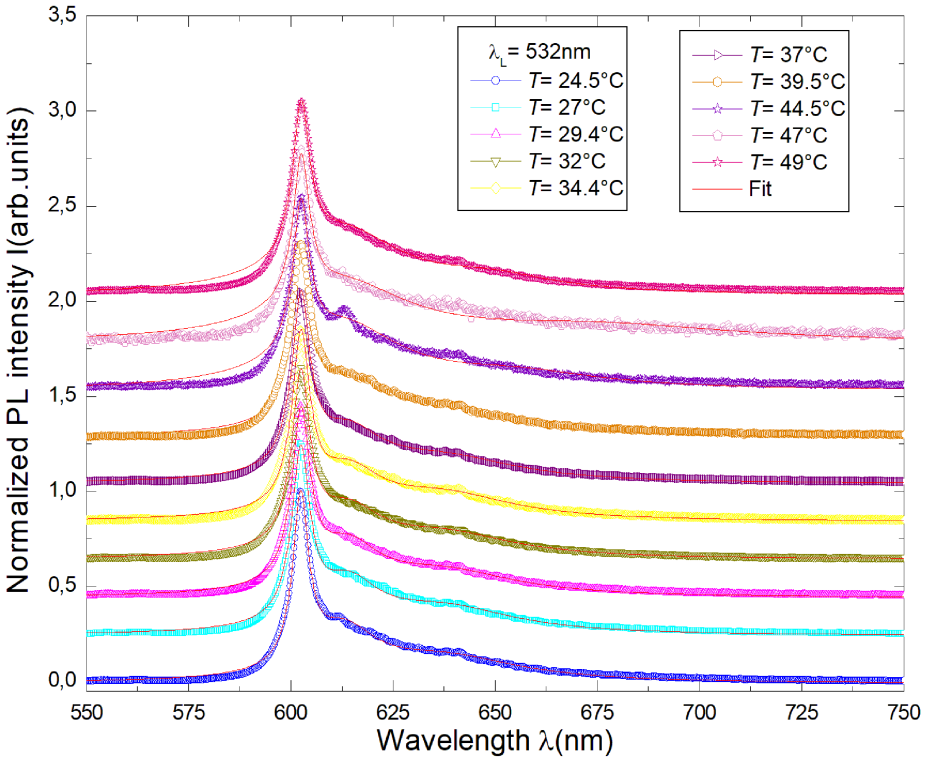

Figure 42: Photoluminescence spectrum of GeV centers, taken at 10 different temperatures with ≈ 2.5°C steps together with the fits.

The changes of the GeV ZPL, i.e. the associated λ_C vs the temperature are plotted in Figure 43. The fit curve describing λ_C, according to Equation 8 possesses parameter $A = 4.9581 \times 10^{-8} \pm 1.7428 \times 10^{-8}$ eV/K^2. Standard deviation error bars for data points are very small but still visible.

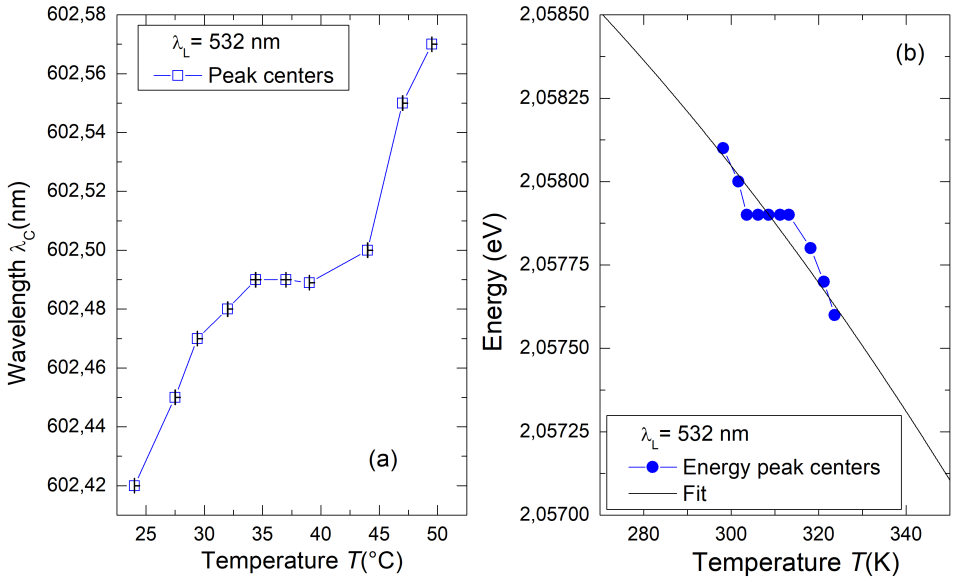

Figure 43: (a) Plot of GeV flourescence central wavelength vs temperature. (b) Plot of GeV flourescence energy central peak vs temperature with the fit.

For comparison purposes, presented are also the results that are not normalized (no background subtraction). The reason comes from the fact that this method of measuring temperature has an aim to be used for temperature control in cells. When working with cells and any type of tissue, many factors play a significant role. One of them is the time of exposure to irradiation that can induce cell degradation. We want to work efficiently and as fast as possible, as in a case when a resistance thermometer is used. A temperature sensor should be as effective as possible. Indeed, results collected and analyzed in this work, prove that background measurements are not necessary for analysis. Results are shown in Figures 44 and 45.

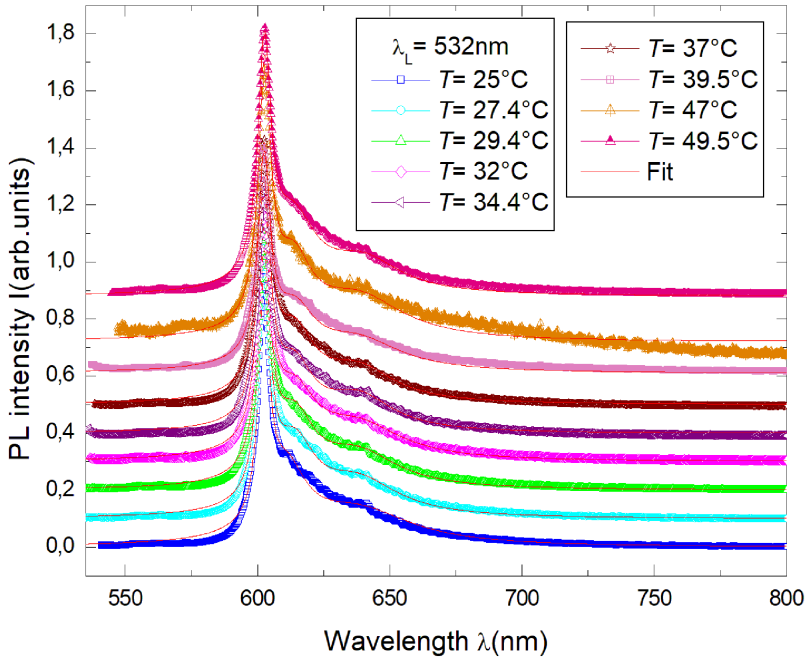

Figure 44: Photoluminescence spectrum of GeV centers, taken at 9 different temperatures with $\approx$ 2.5°C steps together with the fits. No background subtraction.

The fit curve describing λ_C, according to Equation 8 possesses parameter $A = 7.5184 \times 10^{-8} \pm 1.2121 \times 10^{-8}$ eV/K^2 (Fig.45). According to fits done to both results, one with background subtraction and one without, leads us to conclude that the difference in shape of the curve and the value of the slope comes from the contribution of the temperature dependent phonon sidebands, more specifically, from the, probably, biggest contaminant in diamond, Nitrogen. With the background subtraction we are omitting this contribution. Analysis shows that even without the use of background subtraction, one can still very nicely quantify the change of the main peak that comes with the temperature increase and fit it with a function which describes the changes in a very good matter.

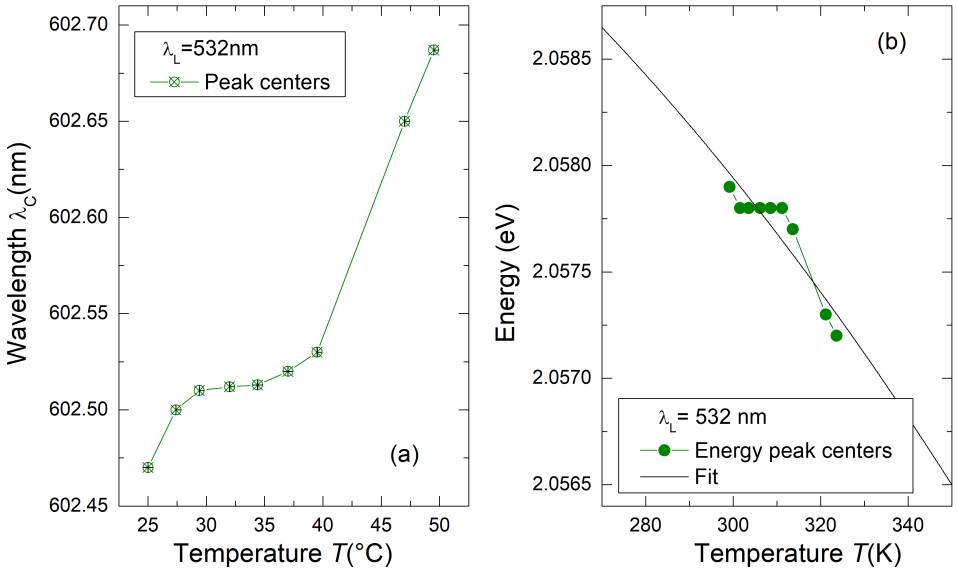

Figure 45: (a) Plot of GeV flourescence central wavelength vs temperature. (b) Plot of GeV flourescence energy central peak vs temperature with a fit done with Eq.8. No background subtraction results.

The results obtained using blue laser are presented in Figure 46, together with the fits. As before, three Lorentzian functions were used, as they allow the most stable fit. The results are, according to the conclusion made above, not subtracted with the background.

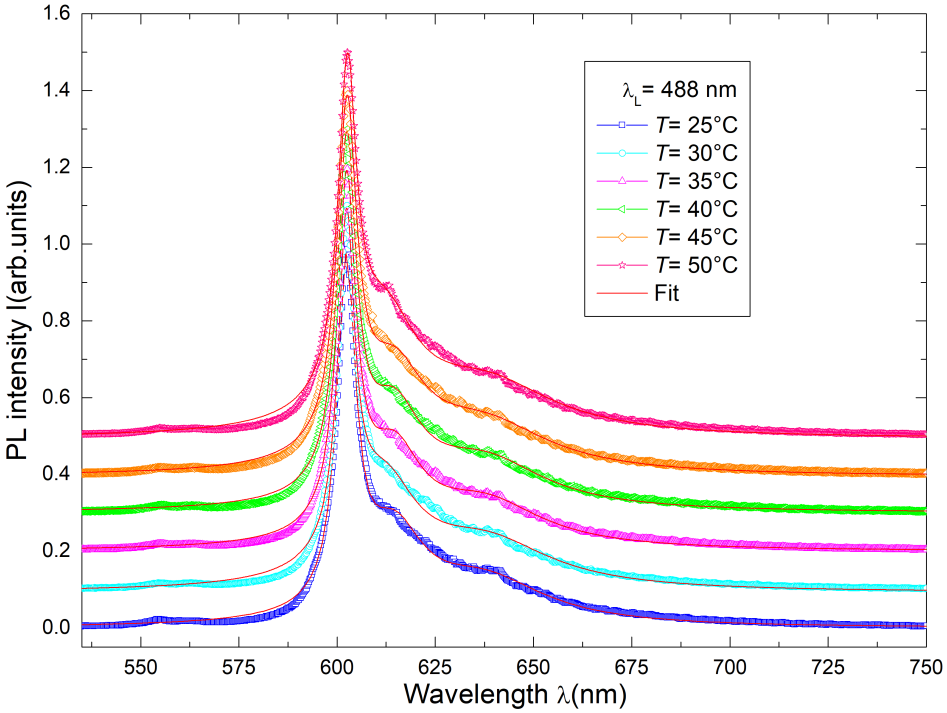

Figure 46: Photoluminescence spectrum of GeV centers taken at 6 different temperatures with 5°C steps together with the fits.

The fit curve describing λ_C, according to Equation 8 possesses parameter $A = 9.0726 \times 10^{-8} \pm 1.2668 \times 10^{-8}$ eV/K^2 (Fig. 47).

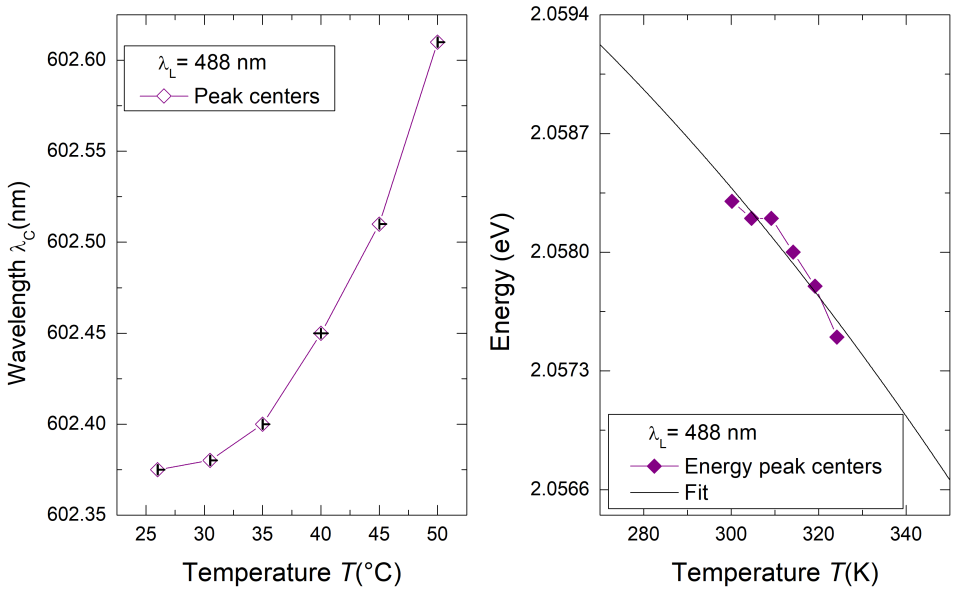

Figure 47: (a) Plot of GeV fluorescence central wavelength vs temperature. (b) Plot of GeV fluorescence energy central peak vs temperature with a fit done using Eq.8.

In order to compare the PL results using two excitation wavelengths (532 nm and 488 nm), together with the PL results belonging to two extreme temperatures (25°C and 50°C) plots are made and shown in Figures 48 and 49.

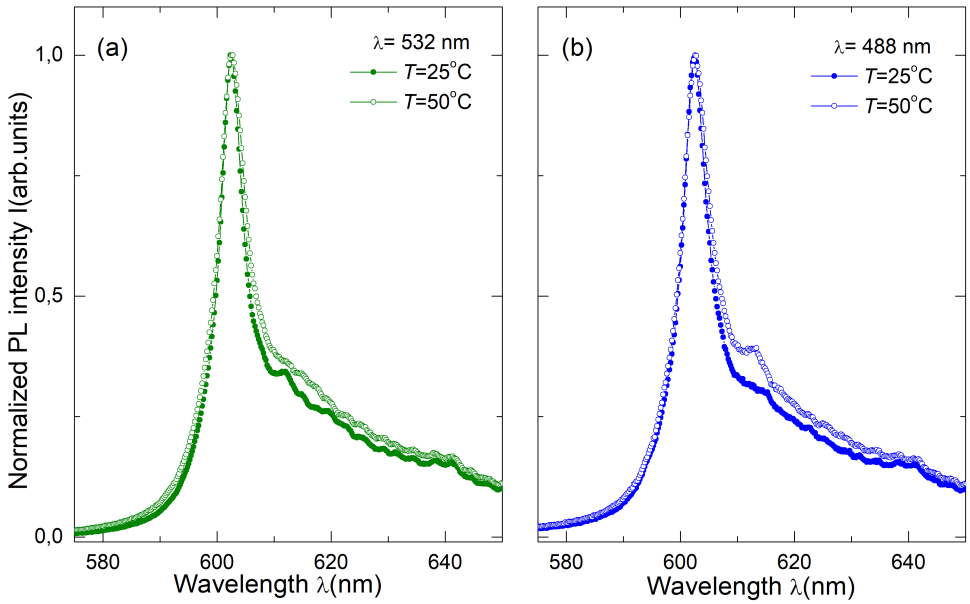

Figure 48: Comparison of the PL results obtained for the two extreme temperatures. In (a) for the green laser and in (b) for the blue laser.

From Figure 48, it is evident that the temperature influences the main peak position and also the phononic sideband for both λ_L used in the experiment. This is expected, because by increasing the temperature we excite more phonons.

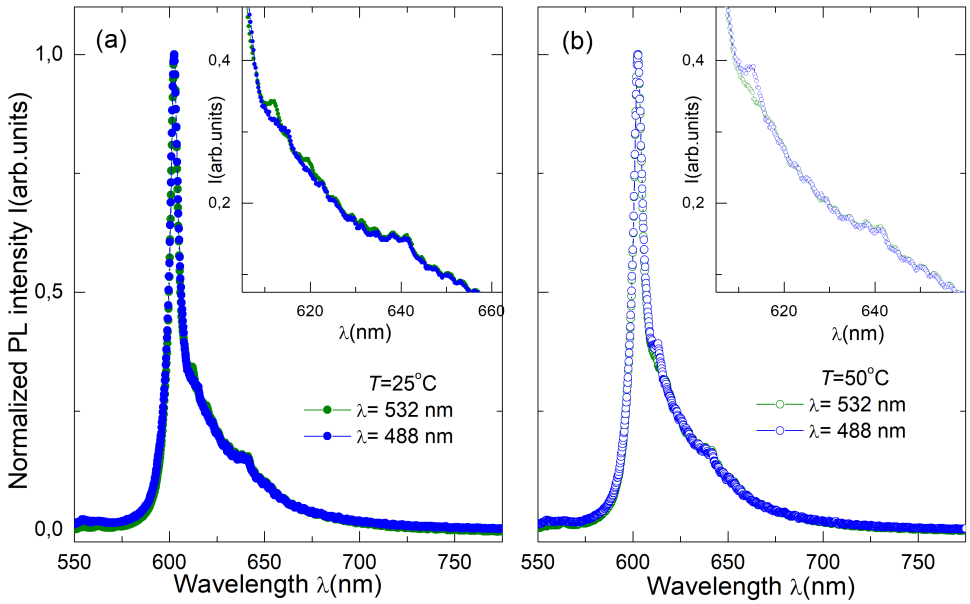

Figure 49: Comparison of PL spectra obtained with two different wavelengths. In (a) $T = 25°C$ and (b) $T = 50°C$. The insets, a zoomed-in region is shown where the difference in phononic sidebands is evident.

In Figure 49, we have compared the PL spectra at two extreme temperatures investigated in this work. We can observe that the use of λ mainly affects the phonon sideband, but not in way that the ZPL is also modified. In the inset are shown the regions of clear difference between the mentioned sidebands.

4.2.3 Magnesium Vacancy Centers

Magnesium Vacancy is not a well-known and described center in the literature, neither theoretically or experimentally. For this reason, in this work, it was investigated with both green and blue laser in order to explore if there is some correlation with the wavelength used.

Firstly, and similar as before, photoluminescence spectra obtained using green laser for all temperatures investigated in this work, together with the fits, are shown in Figure 50. These fits are done using four Lorentzian function, because we wanted to understand the behaviour of the whole spectra. In order to investigate this center as well as possible, we are again showing

the difference between normalized spectra with the background subtraction (Fig. 50) and the one without it (Fig. 53).

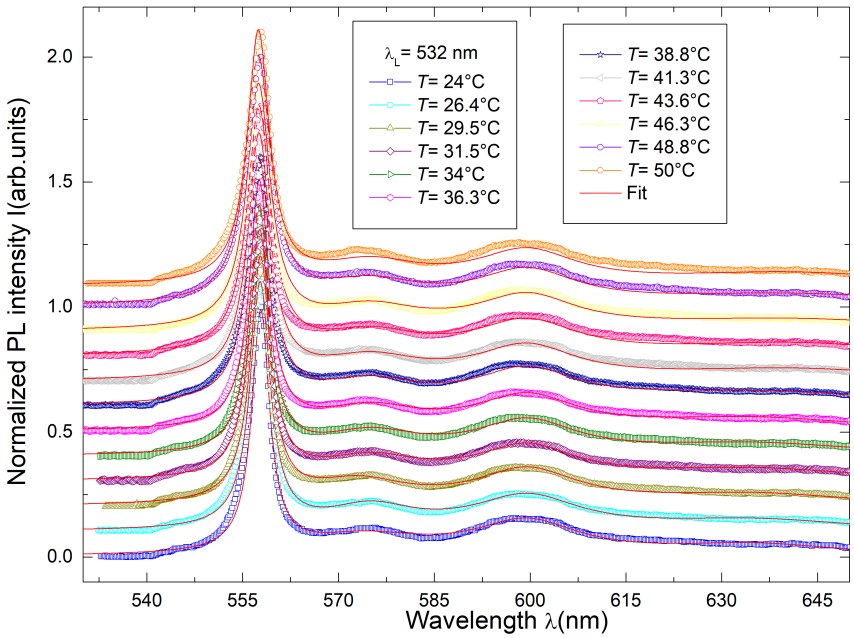

Figure 50: Photoluminescence spectrum of MgV centers, taken at 12 different temperatures with ≈ 2.5°C steps together with the fits. Background is here subtracted.

In order to fit the central wavelength shift, the model described in Section 2.3 was used. Even though the modified Varshni model deals with a large range of temperatures, in this work, it is confirmed that the same equation perfectly describes the results obtained in a small range of temperatures. The fit curve describing λ_C, according to Equation 8 possesses parameter $A = -1.51 \times 10^{-7} \pm 0.0938 \times 10^{-7}$ eV/K^2 (Fig. 51). To remark, for MgV centres we need a negative A parameter, which is unusual if we compare it to the above results and also with those from the literature belonging to other types of color centers, we will discuss about this finding later.

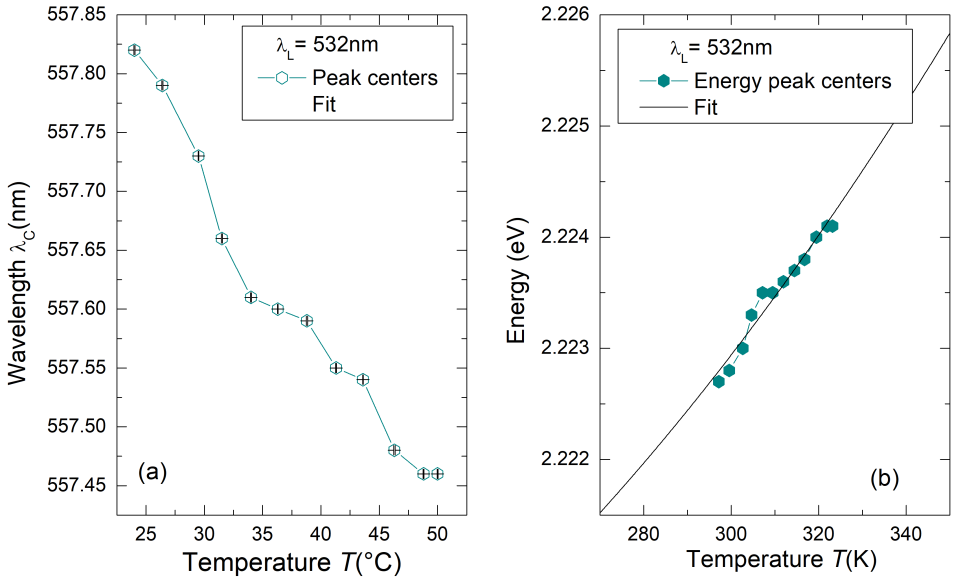

Figure 51: (a) Plot of MgV flourescence central wavelength vs temperature. (b) Plot of MgV flourescence energy central peak vs temperature with the fit done using Eq.8.

For comparison and curiosity purposes, we have also plotted the central wavelength shift with the temperature by fitting our spectra with two Lorentzian functions, which takes into account the main peak and one phonon sideband, which contributes more to the final shape of the ZPL. Results are shown in Figure 52, and the fit curve describing λ_C, according to Equation 8 possesses parameter $A = -1.4624 \times 10^{-7} \pm 0.12336 \times 10^{-7}$ eV/K^2. The results obtained, confirm our hypothesis that for analysis one should use at least two Lorentzian functions to describe the central wavelength shift.

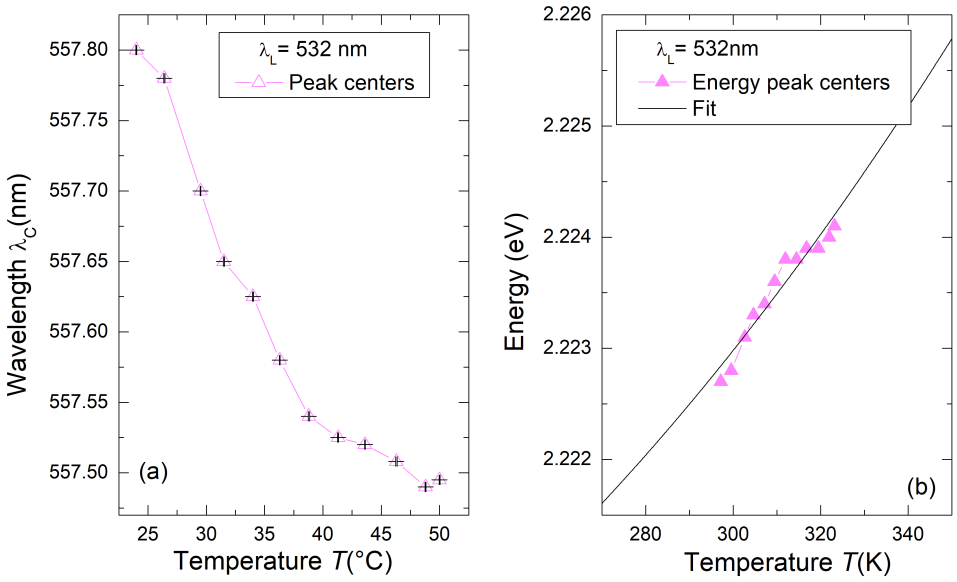

Figure 52: (a) Plot of MgV flourescence central wavelength vs temperature. (b) Plot of MgV flourescence energy central peak vs temperature with the fit done using Eq.8.

Data are also analysed without the background subtraction (Fig. 53), to show the difference and to understand the contributions of the phonon sidebands in a better way, since MgV is a fairly new discovered color center that is not yet well investigated. Here, two Lorentzian functions are used for fitting, as confirmed reasonable.

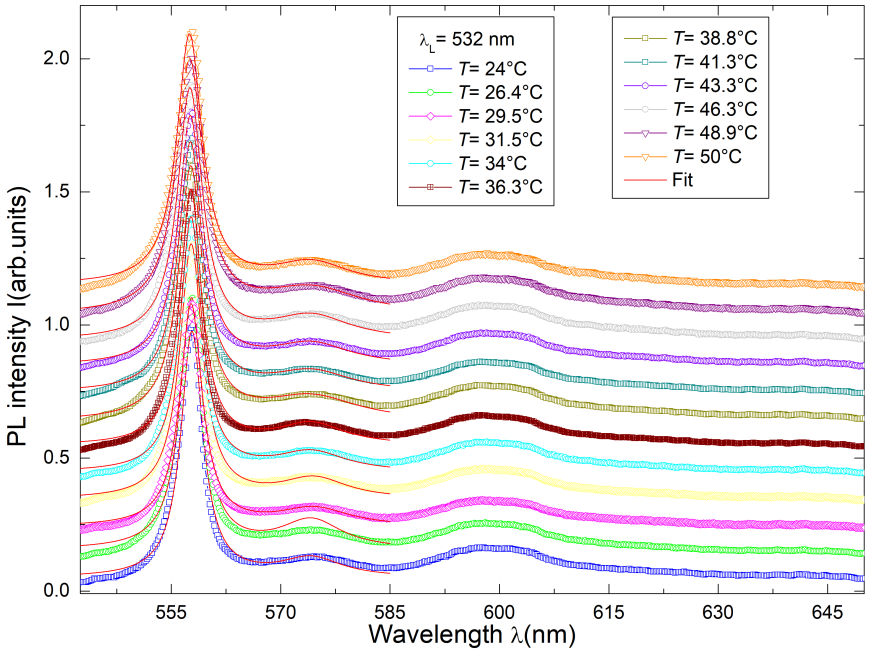

Figure 53: Photoluminescence spectrum of MgV centers, taken at 12 different temperatures with $\approx$ 2.5°C steps together with the fits. No background subtraction. To remark, fits were done using two Lorentzian functions.

The fit curve describing λ_C, according to Equation 8 possesses parameter $A = -1.2472 \times 10^{-7} \pm 0.074164 \times 10^{-7}$ eV/K^2.

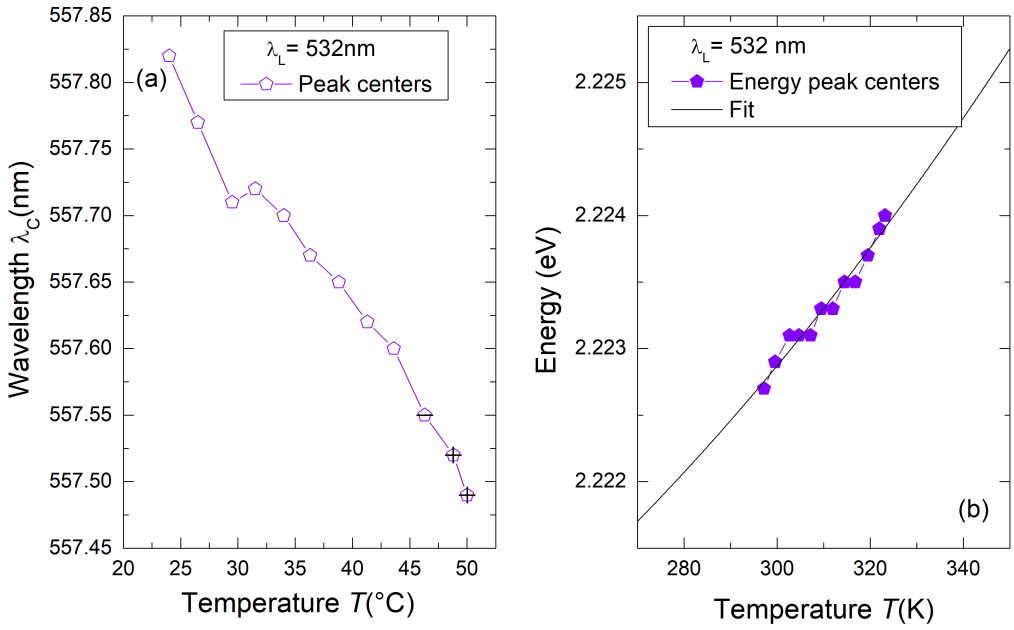

Figure 54: (a) Plot of MgV flourescence central wavelength vs temperature. (b) Plot of MgV flourescence energy central peak vs temperature with the fit done using Eq.8.

When we compare the results obtained from Figure 52 and 54, we can clearly conclude that the background subtraction is not necessary, under condition that analysis should include at least two Lorentzian functions that takes into account the main peak and the first phonon sideband. This makes the future cell temperature investigation very fast and effective. These results are already a hint that MgV is more convenient as a temperature sensor then NV or GeV.

In the Figure 55, PL spectra recorded with the blue laser is shown. Fits are done using two Lorentzian function.

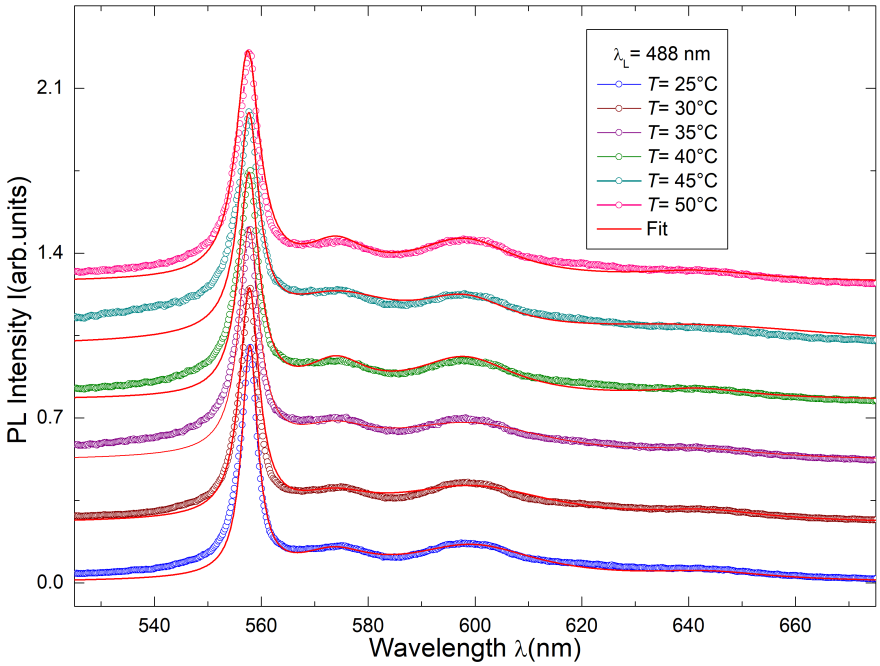

Figure 55: Photoluminescence spectrum of MgV centers, taken at 6 different temperatures with 5°C steps together with the fits.

The fit curve describing λ_C, according to Equation 8 possesses parameter $A = -1.4172 \times 10^{-7} \pm 0.25728 \times 10^{-7}$ eV/K^2 (Fig.56).

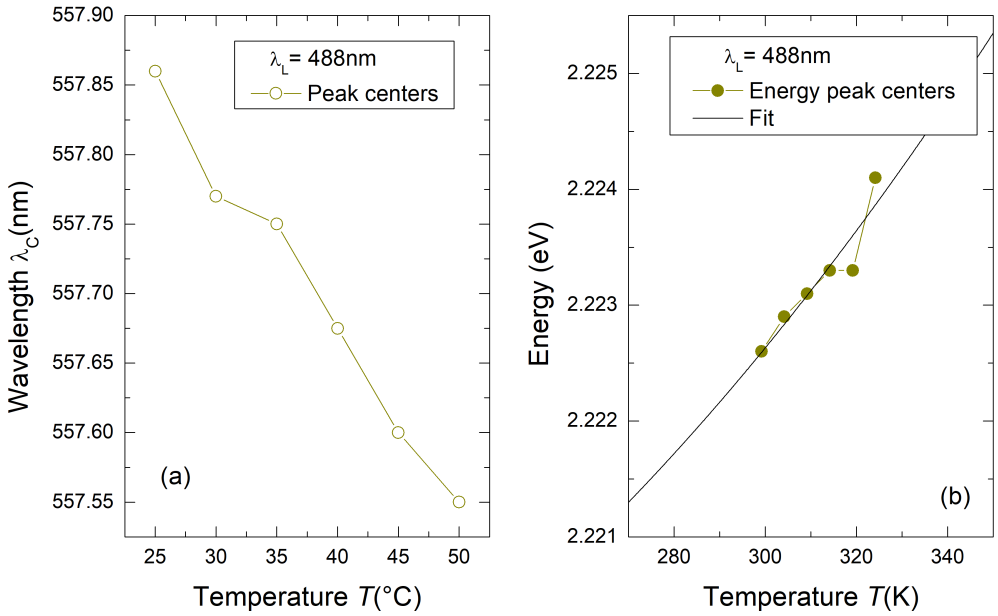

Figure 56: (a) Plot of MgV fluorescence central wavelength vs temperature. (b) Plot of MgV fluorescence energy central peak vs temperature with the fit done using Eq.8.

Literature had shown that for the most know color centers, NV [16], GeV [10] and SiV [22] by increasing the temperature, the ZPL moves to higher λ_C values, which is called a red shift. Surprisingly, the investigated MgV center is showing a decreasing of central peak by temperature increase, know as a blue shift. Usually, blue shift is observed as consequence of size change, i.e. the characteristic peak, PL or Raman, shows an unique value in the bulk, after the sample size change in nm range, that unique peak position changes showing a blue shift. Later when the nano-sized sample is measured by increasing the temperature, the new position of the unique peak shows a red shift. Our MgV center is very unusual because of two reasons, one, the sample is the bulk, and second, by increasing the temperature we observe the blue shift. Because of lacking of theoretical studies regarding the structure of the MgV centres, and taking into account that Germanium and Silicon form a divacancy inside the diamond, where one carbon atom is substituted with the corresponding element connected with two vacancies, it makes us to suppose that Magnesium forms a different type of vacancy inside the diamond. By increasing the temperature, the local environment of the MgV

centre is changed in such a way that ZPL shifts in blue instead of a red shift.

As before, in order to compare the two excitation wavelengths (532 nm and 488 nm), together with the two extreme temperatures (25°C and 50°C) plots are made and shown in Figures 57 and 58.

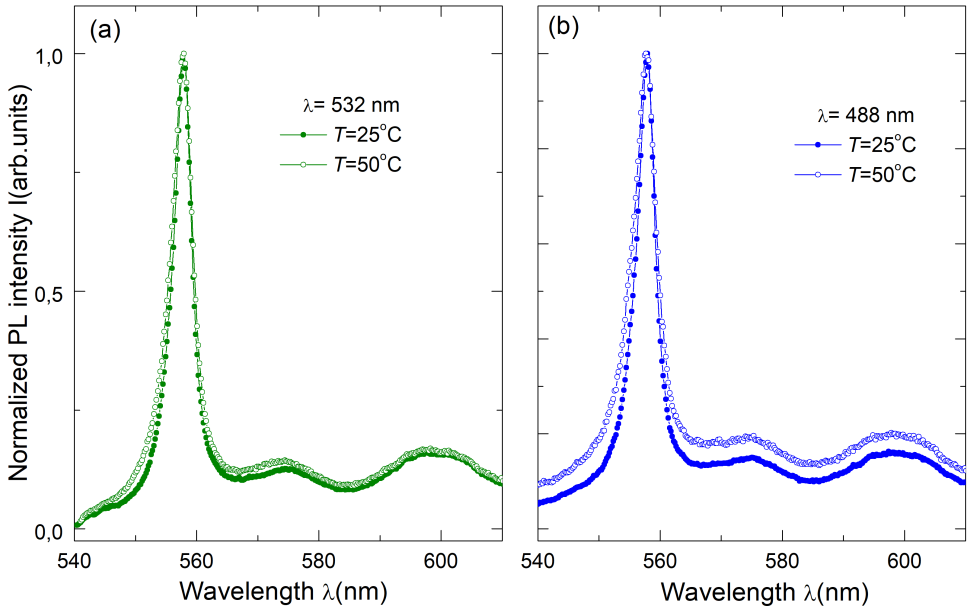

Figure 57: Comparison of PL spectra of the green laser. In (a) for the green laser (b) for the blue laser.

From Figure 57, we can conclude that temperature indeed influences the shift of the central peak. In the case of blue laser, this behaviour is more evident, because we are exciting more phononic regions with this particular wavelength.

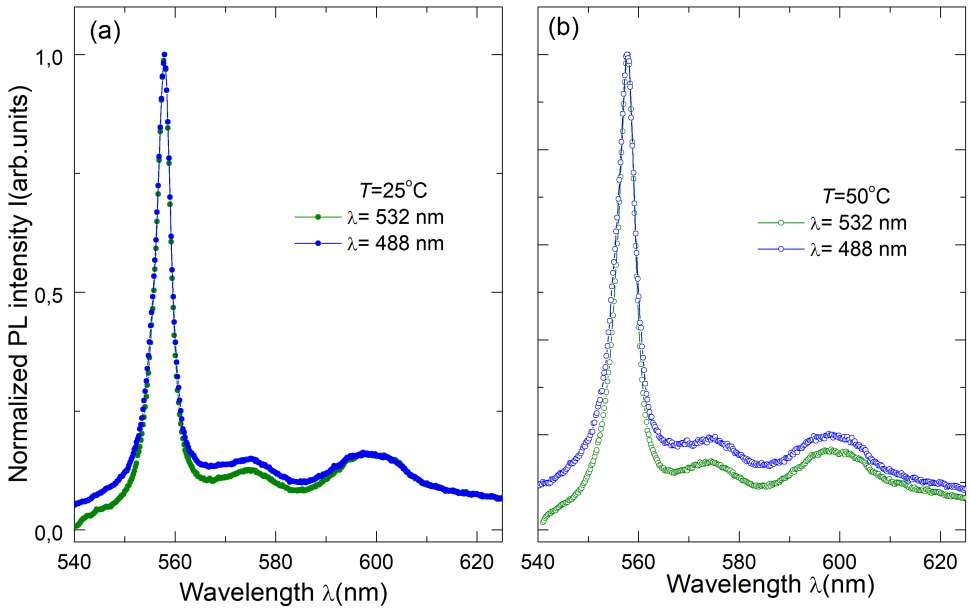

Figure 58: Comparison of PL spectra obtained with two laser wavelengths. In (a) for $T = 25°C$ and in (b) for $T = 50°C$.

In Figure 58, we have compared the PL spectra at two extreme temperatures investigated in this work. It clearly shows that the choice of λ affects the phonon sidebands in a prominent way, but for analysis purpose of the ZPL it is not fully decisive.

4.3 Discussion of Results

Finally, after all the data has been analyzed and presented, we can make important conclusions, starting with, for future determination of temperature inside the cells, one does not need to take into account the background subtraction, since longer exposure to radiation is harmful for the cell or a tissue. Support of our assumption is given in Figure 59 where one can observe that the shift of the central peak influenced by the temperature is not significantly affected by the background subtraction.

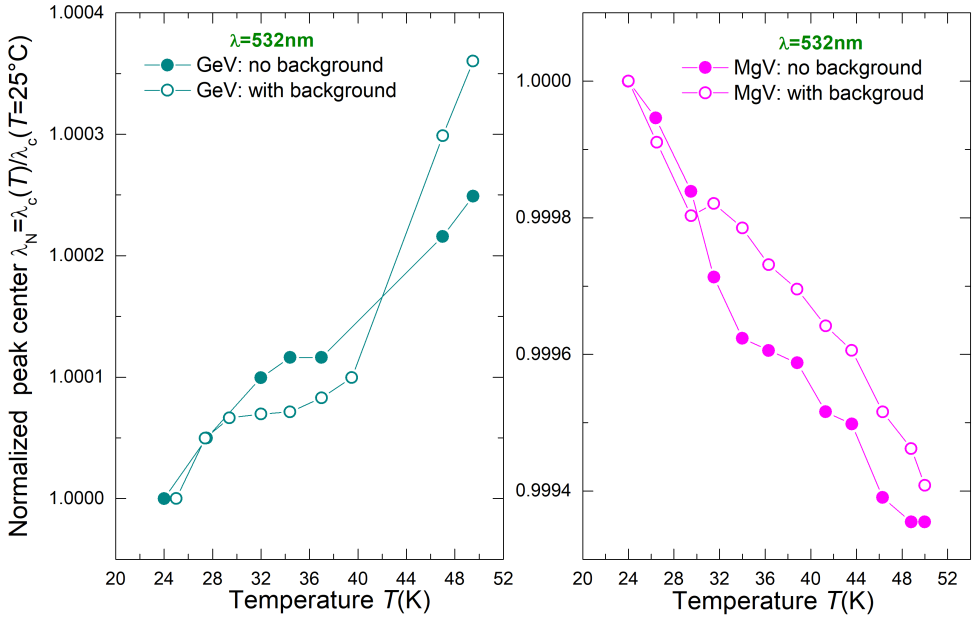

Figure 59: Comparison of central peak temperature induced shift of GeV and MgV for green laser measurement. Data were normalized for comparison purposes.

At this point, I will introduce a common analysis technique used in the world of thermometry. Standard technique of determination of the ability and quality of the resistor thermometer (e.g. PT100 that was used in this work), is given by $R(T) = R_B[1 + \alpha(T - T_B)]$, where R_B is the the resistance at the temperature $T = T_B$ and α the so called temperature coefficient of the resistance. The α of conventional temperature sensor as PT100 is $\approx 38.5 \times 10^{-4}$/K. Therefore, the coefficient α is the most important parameter to be taken into account for application purposes. We have applied similar procedure to our color centers and determined the α coefficient, which tells us about the quality of our thermometer. Equation has been modified and now reads, $\lambda_C(T) = \lambda_{C,B}[1 + \alpha(T - T_B)]$, where $\lambda_{C,B}$ is the central wavelength peak at the temperature $T = T_B$. Results are given in Table 2. When we look at the literature that is dealing with color centers in diamond for thermometry purposes, one notices that this type of description of the quality of thermometer is not done, and no comparison with the usual thermometer can be found. In this work, this was done in order to make future investigations that will be done by biophysicists and engineers, easier. Rea-

soning comes from the fact, that when dealing with thermometers, one needs a unique language of units and parameters that is common in the scientific world and therefore easily understandable.

Color Centers	$\alpha_{\lambda=532\ \mathrm{nm}}[1/\mathrm{K}]$	$\alpha_{\lambda=488\ \mathrm{nm}}[1/\mathrm{K}]$
NV^-	-	$7.4 \times 10^{-6} \pm 0.4 \times 10^{-6}$
NV^0	-	$3.4 \times 10^{-5} \pm 0.4 \times 10^{-5}$
GeV	$9.8 \times 10^{-6} \pm 0.6 \times 10^{-6}$	$6.7 \times 10^{-7} \pm 0.6 \times 10^{-7}$
MgV	$2.7 \times 10^{-5} \pm 0.15 \times 10^{-5}$	$2.2 \times 10^{-5} \pm 0.15 \times 10^{-5}$

Table 2: Calculated α values for all investigated samples.

In order to justify that our method is adequate, we have extracted the data from the literature and did the similar analysis. For results shown in Figure 19 (b) [18], dealing with GeV centers as thermometers, we calculated the α parameter and obtained the value of $\alpha \approx 12.5 \times 10^{-6} 1/K$, which is in almost complete agreement with our results. This validates our used method. Moreover, it is very worthy to remark that the α of the MgV centers is one order greater than the GeV centers, which implies that it performs as a better thermometer in comparison with the GeV centers.

In order to give reasons to our statement that the MgV center is a better candidate than the GeV center for thermometry purposes, we have plotted in Figure 60 (b) the estimated half width ($\Delta\lambda_W$) vs temperature, from the main peak of the PL spectrum without background subtraction. As example we can see the PL spectrum of the MgV and GeV center in Figure 60 (a) measured at $T = 25°\mathrm{C}$. From the plot $\Delta\lambda_W$ vs the temperature we can observe that the $\Delta\lambda_W$ of the MgV centers is almost the half of the GeV center. This indicates how well defined PL peak of the MgV center is, and so satisfies an important criteria for thermometry, it can be used even at higher temperatures. As already discussed, the λ_C position decreases by increasing the temperature, the so-called blue shift, but now we also observe that the $\Delta\lambda_W$ increases by increasing the temperature, which according to our knowledge should be expected, because the broadening of the $\Delta\lambda_W$ is a consequence of the lattice vibration or in other words the influence of the phonons. So, we can assume that the blue shift should be mainly a result of the electronic transition properties itself with addition to the static local structure.

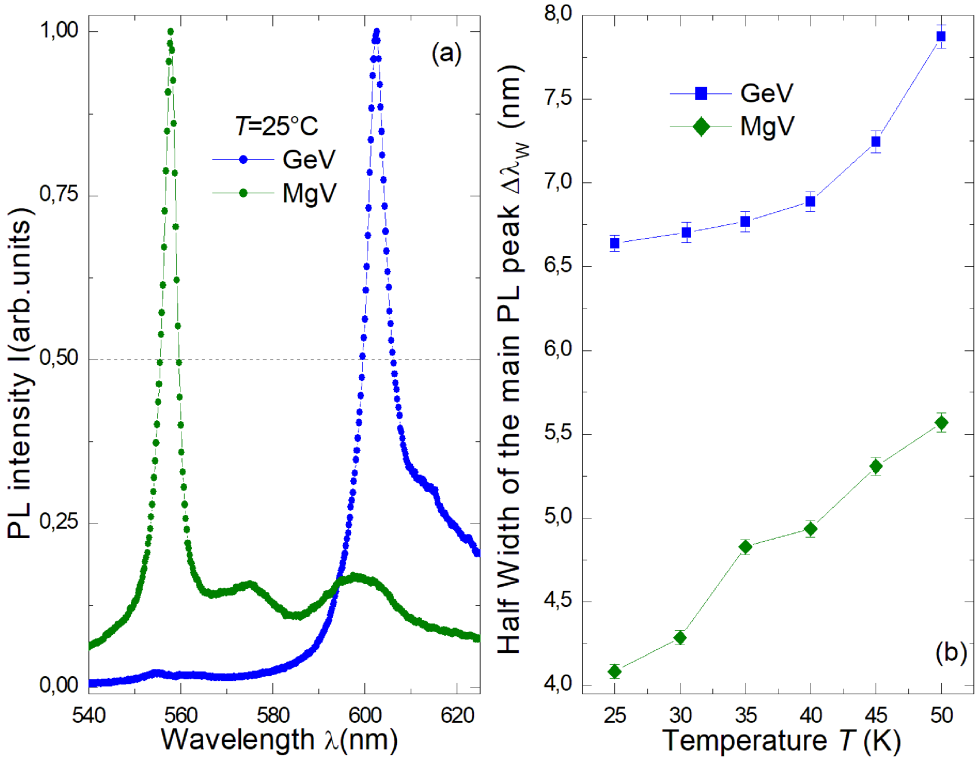

Figure 60: In (a) the photoluminescence of GeV and MgV centers at $T = 25°C$, the dashed horizontal line shows where we determined the $\Delta\lambda_W$. In (b) the $\Delta\lambda_W$ vs the temperature. The $\Delta\lambda_W$ were estimated from the PL without background subtraction.

5 Conclusion and Outlook

During this Master work, color centers in diamond for thermometry purposes were investigated. These color centers include Nitrogen Vacany centers, Germanium Vacany centers and Magnesium Vacany centers. Ion implantation is the method of choice for a high throughput screening of named chemical elements. In this work, different energies were used (5 keV, 15 keV, 40 keV, 80 keV) for production of centers at different depths. From the results of the NV centers, we can conclude that the ones implanted with the high energy give out the best results, therefore we have decided to produce the rest of the centres using the highest energy possible. In order for a color center to be produced, annealing is a necessary step and it depends on the element implanted. Diamond sample in this work was annealed for 4 h at 800°C for creation of NV centers and 4 h at 1200°C for creation of GeV and MgV centers. After annealing, the sample was cleaned in an passive oxygen plasma chamber, which removed most of the carbon based material from the surface of the diamond. Additional cleaning was done using the process of chemical cleaning. Photoluminescence measurements that followed, took place with the home-made confocal microscope. Two laser wavelengths (532 nm and 488 nm) were used for investigation. PL measurements verified that we were successful with the generation of the desired color centers.

The temperature controller together with the self-developed temperature stage, proved to be an essential part of this work that had allowed us to perform the temperature measurements in the desired range, namely between 20°C and 50°C, even though the temperature controller can easily be used up to 125°C. Range was chosen in this way because the aim of these color centers for the future, is the determination of temperature inside cells, which is a process that requires good temperature resolution and small sensor volumes necessary for accurate, high-resolution *in-vivo* thermometry.

GeV and NV temperature dependent photoluminescence measurements have been used as a test of the performance of the said temperature controller, and the obtained results are in perfect accordance with the previous literature experimental results.

MgV is a fairly new discovered color center, which has not been described theoretically, or enough experimentally investigated such that we could understand its structure inside the diamond. Even when considering this fact, MgV is, in this work, proven to be a better temperature sensor than GeV and NV, this conclusion is supported by the determined α coefficient. Com-

parison between GeV and MgV PL spectra for two lasers and two extreme temperatures is shown in Figures 61 and 62, in them we can easily see that the ZPL of the MgV centers is more defined than the one belonging to GeV centers. This fact makes it reasonable to use MgV centers in thermometry and, in all likelihood, at even higher temperatures than investigated in this work. Fit of the central wavelength peak temperature induced shift can be perfectly described with the modified Varshni model, which is know from the literature and used to describe other types of centres in diamond. Comparison of these results for all investigated color centers and the two used wavelengths is given in Figure 63. When looking at this Figure, we can see that the MgV centres manifest the highest change in the central peak shift with the temperature. One can argue that similar change can be observed in NV^0 centres, but here the contribution of the phononic sidebands is extremely high and it influences the peak shift significantly, and the real half width is almost impossible to correctly determine (see Figure 40). Peak of MgV ZPL is, on the other hand, very well defined and it is easier to quantify its shift with the temperature. In this work we have also discovered that the shift of the λ_C with the temperature of the MgV center is unusual, i.e. it's value decreases with the temperature. For example, the λ_C vs the temperature in NV, GeV and SiV centers increases [19,21,55], or in other words, follows a so-called red shift, i.e by increasing the temperature, the value of the λ_C increases. Blue shift, i.e. the shift of the characteristic PL peak or Raman peak is well know when a material is nano-sized. Blue shift is know for example in the Raman peak of sub 10 nanometer nanodiamond [56], and it is well understood as consequence of the modified phonon confinement effect. A blue shift was also observed in SiV centers in nanodiamonds [57] and supported by *ab initio* Kohn–Sham density functional theory. The theory explains that the ZPL blue shift in SiV is due to hydrostatic pressure [57], whereas uniaxial strain causes larger red shift with different magnitudes depending on the direction of the strain. To emphasize, blue shifts were observed as a consequence of a size effect or as in SiV because of size effects with addition of pressure, and the blue shift is referred to the shift of the ZPL peaks with respect to the ZPL peaks observed in the bulk. When the nanosized sample is later heated, the ZPL follows the red shift again. Our case is more complicated, because we observe a blue shift by increasing the temperature and considering our sample is bulk, we can not attribute this change to a size and/or confinement effect. Other explanation could be some local hydrostatic pressure, which could possibly exist in our sample, but an

increase in the temperature should reduce this pressure by relaxation of the lattice and doing so, induce a red shift, so we can discard that the blue shift of the ZPL can be explained by pressure inside the sample. The effect of the lattice oscillation by increasing of the temperature indeed exists and it is observed in the $\Delta\lambda_C$, i.e. this value increases by increasing the temperature (Fig.60). To conclude, the blue shift observed in the ZPL of the MgV centers by the temperature, remains as an open question to be investigated in the future both experimentally and theoretically.

Lastly, we recommend the continuation of investigation of the MgV centers inside the bulk diamond and their implantation in the nanodiamonds. For this we have three main reasons. First, very small half width which suggests that MgV centers can be used as thermometers at much higher temperatures than other know color centers. Second, the rapid change of λ_C with the temperature characterized by the α value and finally, the observed unusual blue shift. Our experimental results and the analysis of those, show that MgV are indeed an excellent candidate for the *in-vivo* thermometry. During the experiments, and subsequent analysis, we have shown that we can reproduce the results from the literature, but it is highly recommended to increase the resolution of the camera integrated in the confocal microscope, as the better resolution will be necessary for the future investigation in nanodiamonds.

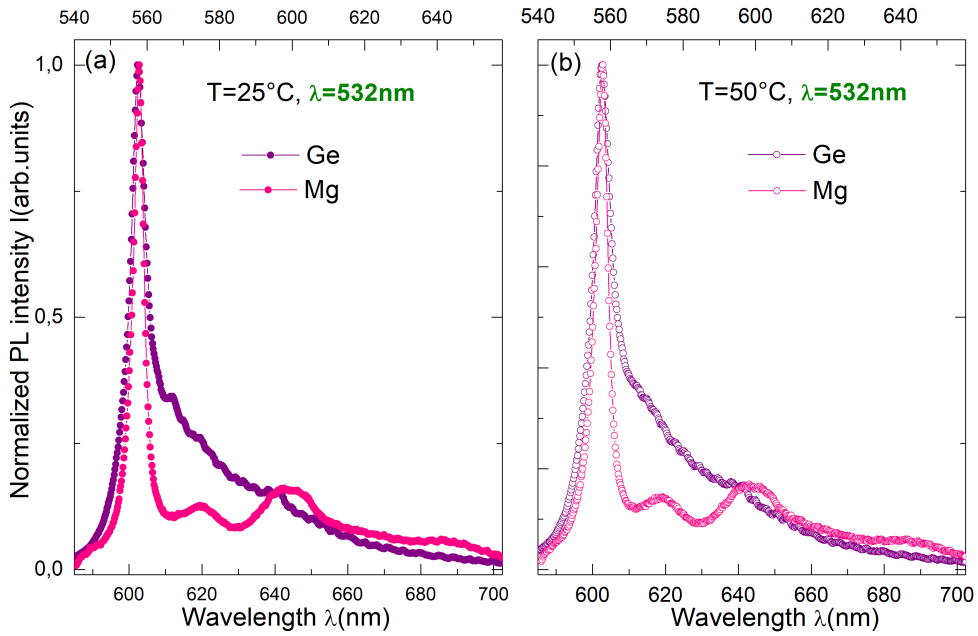

Figure 61: Comparison of PL spectra of the (a) $T = 25°C$ and (b) $T = 50°C$ of GeV and MgV centers investigated with green laser. Lower x-axis belongs to GeV and the upper to the MgV centres.

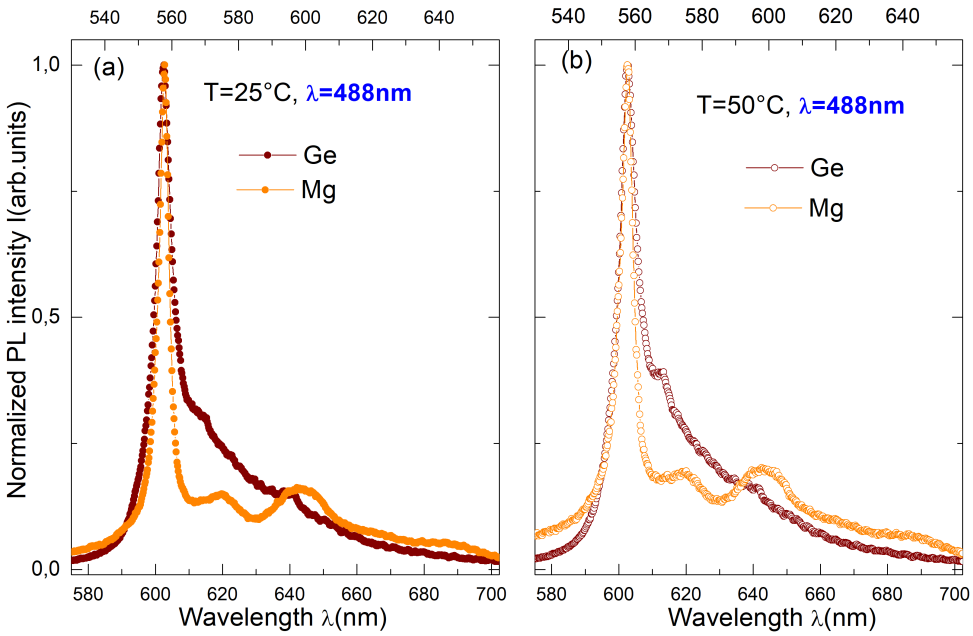

Figure 62: Comparison of PL spectra of the (a) $T = 25°C$ and (b) $T = 50°C$ of GeV and MgV centers investigated with blue laser. Lower x-axis belongs to GeV and the upper to the MgV centres.

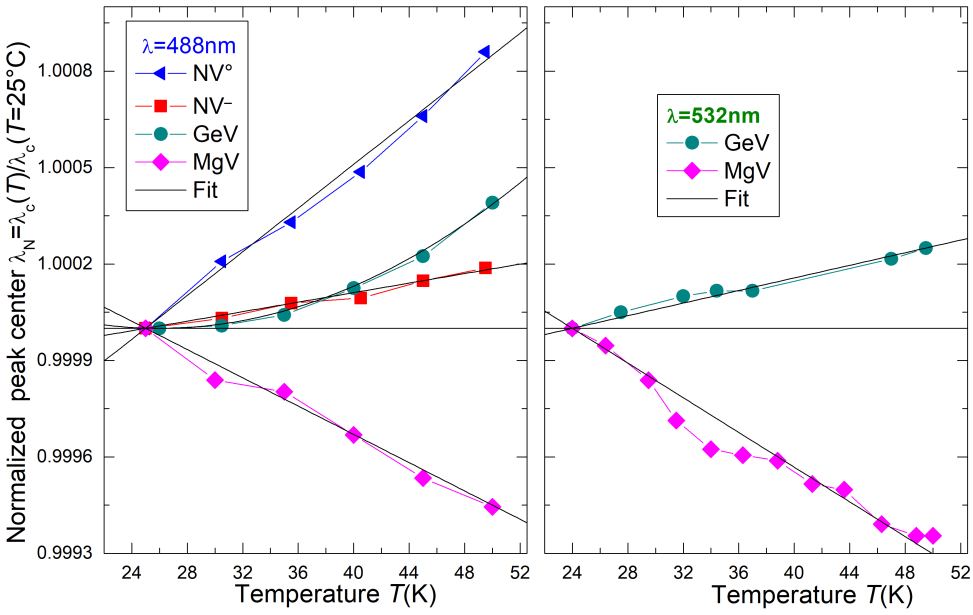

Figure 63: Comparison of central peak shifts of all investigated samples together with the corresponding wavelength.

6 References

[1] https://en.wikipedia.org/wiki/Dresden_Green_Diamond

[2] https://glossary.periodni.com/glossary.phpen=sp3hybridorbitald

[3] http://www.chm.bris.ac.uk/motm/diamond/diamondh.htm

[4] Fundamentals of the Physics of Solids, Jeno Solyom, Springer (2007)

[5] https://www.gia.edu/gems-gemology

[6] https://www.degruyter.com/document/doi/10.1515/nanoph-2019-0154/html

[7] J. R. Maze, A. Gali, E. Togan, Y. Chu, A. Trifonov, E. Kaxiras, und M. D. Lukin, "Properties of nitrogen-vacancy centers in diamond: The group theoretic approach", New Journal of Physics, 13(2):025025

[8] R. Schirhagl *et.al*, "Nitrogen-vacancy centers in diamond: nanoscale sensors for physics and biology", Annual Review of Physical Chemistry 65(1)

[9] P. Siyushev *et.al*, "Optical and microwave control of germanium-vacancy center spins in diamond", PHYSICAL REVIEW B 96, 081201(R) (2017)

[10] Takayuki Iwasaki *et.al*, "Germanium-Vacancy Single Color Centers in Diamond", Scientific Reports, 5:12882

[11] https://en.wikipedia.org/wiki/Magnesium

[12] Tobias Lühmann *et.al*, "Screening and engineering of colour centres in diamond" 2018 J. Phys. D: Appl. Phys. 51 483002

[13] https://www.wikilectures.eu/w/Thermometry

[14] https://qsstudy.com/physics

[15] https://physicsabout.com/types-of-thermometer/

[16] G. Kucsko *et.al*, "Nanometre-scale thermometry in a living cell", NATURE, Vol 500, 2013

[17] Chen *et.al*, "Temperature dependent energy level shifts of nitrogen-vacancy centers in diamond", Appl. Phys. Lett. 99, 161903 (2011)

[18] Jing-Wei Fan *et.al*, "Germanium-Vacancy Color Center in Diamond as a Temperature Sensor", ACS Photonics 2018, 5, 765−770

[19] Cong-Cong Li *et.al*, "Temperature dependent energy gap shifts of single color center in diamond based on modified Varshni equation", Diamond & Related Materials 74 (2016)119–124

[20] `https://www.thorlabs.com/index.cfm`

[21] Mingyang Yang *et.al*, "A Diamond Temperature Sensor Based on the Energy Level Shift of Nitrogen-Vacancy Color Centers", Nanomaterials 2019, 9, 1576

[22] Stefan Häußler *et.al*, "Photoluminescence excitation spectroscopy of SiV and GeV color center in diamonds", New J. Phys. 19 063036

[23] W. Doherty *et.al*, "The nitrogen-vacancy colour centre in diamond", Physics Reports Volume 528, Issue 1

[24] J R Maze *et.al*, "Properties of nitrogen-vacancy centers in diamond: the group theoretic approach", New Journal of Physics 13 (2011) 025025

[25] Robert Chapman and Taras Plakhotnik, "Anomalous saturation effects due to optical spin depolarization in nitrogen-vacancy centers in diamond nanocrystals", PHYSICAL REVIEW B 86, 045204 (2012)

[26] Ke Wei *et.al* , "Temperature-dependent excitonic photoluminescence excited by two-photon absorption in perovskite CsPbBr quantum dots", Vol. 41, No. 16, August 15 2016, Optics Letters

[27] G. Thiering *et.al* , "Color centers in diamond for quantum applications", Semiconductors and Semimetals, ISSN 0080-8784

[28] J.M.Smith *et.al* , "Colour centre generation in diamond for quantum technologies", Nanophotonics 2019; 8(11): 1889–1906

[29] M. W. Doherty *et.al* , "Temperature shifts of the resonances of the NV^- center in diamond", PHYSICAL REVIEW B 90, 041201(R) (2014)

[30] Michael E. Thomas and W.J. Tropf , "Optical properties of diamond", fohns Hopkins APL Technical Digest, Volume 14, Number 1 (1993)

[31] S. Lin *et.al* , "Temperature dependent coherence properties of NV ensemble in diamond up to 600 K", arXiv:2102.12790

[32] M. Alkahtani *et.al* , "Tin-vacancy in diamonds for luminescent thermometry", Appl. Phys. Lett. 112, 241902 (2018)

[33] Fluorescent Nanodiamonds, First Edition. Huan-Chen Chang, Wesley Wei-Wen Hsiao and Meng-Chih Su

[34] V.A.Drebushchak , "Thermal expansion of solids: review on theories", Journal of Thermal Analysis and Calorimetry (2020) 142:1097–1113

[35] G Davies, "Vibronic spectra in diamond", J. Phys. C: Solid State Phys. 7 3797

[36] Romana Schirhagl *et.al* , "Nitrogen-Vacancy Centers in Diamond: Nanoscale Sensors for Physics and Biology", Annu. Rev. Phys. Chem. 2014. 65:83–105

[37] Ariful Haque and Sharaf Sumaiya , "An Overview on the Formation and Processing of Nitrogen-Vacancy Photonic Centers in Diamond by Ion Implantation", J. Manuf. Mater. Process. 2017, 1,6

[38] T. Plakhotnik *et.al* , "All-Optical Thermometry and Thermal Properties of the Optically Detected Spin Resonances of the NV^- Center in Nanodiamond", Nano Lett. 2014, 14, 4989−4996

[39] A. Gali *et.al* , "Ab initio supercell calculations on nitrogen-vacancy center in diamond: Electronic structure and hyperfine tensors", PHYSICAL REVIEW B 77, 155206, 2008

[40] W. Saslow *et.al* , "Band structure and optical properties of diamond", PHYSICAL REVIEW LETTERS, Volume 16, Number 9, 1966

[41] K. Wang *et.al* , "Photoluminescence Studies of Both the Neutral and Negatively Charged Nitrogen-Vacancy Center in Diamond", Microsc. Microanal. 22, 108–112, 2016

[42] Y. P. Varshni, "Temperature dependence of the energy gap in semiconductors", Physica 34, 149-154

[43] B. I. Shklovskii and A. L. Efros, "Electronic Properties of Doped Semiconductors", volume 45 of Springer Series in Solid-State Sciences. Springer, 1 edition 1984.

[44] M. Steiner *et.al*, "Universal enhan- cement of the optical readout fidelity of single electron spins at nitrogen-vacancy centers in diamond" Phys. Rev. B, 81:035205, 2010. 3.1.1, 3.6

[45] W. C. Walker und J. Osantowski, "Ultraviolet optical properties of diamond". Phys. Rev., 134:A153–A157, Apr 1964. 2.1.2

[46] J. F. Ziegler, M. D. Ziegler, und J. P. Biersack, "SRIM - The stopping and range of ions in matter" (2010). Nuclear Instruments and Methods in Physics Research Section B: Beam Interactions with Materials and Atoms, 268(11-12):1818 – 1823, 2010. 19th International Conference on Ion Beam Analysis. 4.1.3

[47] D. Weaire und M. F. Thorpe, "Electronic properties of an amorphous solid. I. A simple tight-binding theory". Phys. Rev. B, 4:2508–2520, Oct 1971. 2.2

[48] L. Robledo *et.al*, "Spin dynamics in the optical cycle of single nitrogen-vacancy centres in diamond". New Journal of Physics, 13(2):025013, 2011. 3.1

[49] H. R. Philipp und E. A. Taft, "Optical properties of diamond in the vacuum ultraviolet". Phys. Rev., 127:159–161, Jul 1962. 2.1.2

[50] J. C. Phillips, "Hybrid excitons in diamond". Phys. Rev., 139:A1291–A1294, Aug 1965. 2.1.2

[51] Arun Madan und Melvin P. Shaw, "The Physics and Applications of Amorphous Semiconductors", Academic Press, 1988. 2.2.2

[52] Takao Sasagawa *et.al*, "A route to tunable direct band-gap diamond devices: Electronic structures of nanodiamond crystals", Journal of Applied Physics 104, 073704 (2008)

[53] Tobias Nöbauer *et.al*, "Creation of ensembles of nitrogen-vacancy centers in diamond by neutron and electron irradiation", arXiv 2013

[54] Zaitsev, A. M. "Optical Properties of Diamond"

[55] K. Dragounova *et.al*, "Determination of temperature dependent parameters of zero-phonon line in photoluminescence spectrum of silicon-vacancy centre in CVD diamond thin films", Journal of ELECTRICAL ENGINEERING, VOL 68 (2017), NO1, 74–78

[56] S. Stehlik *et.al*, "Size and Purity Control of HPHT Nanodiamonds down to 1 nm", J. Phys. Chem. C 2015, 119, 27708−27720

[57] S. Lindner *et.al*, "Strongly inhomogeneous distribution of spectral properties of silicon-vacancy color centers in nanodiamonds", 2018 New J. Phys. 20 115002

Acknowledgements

I would like to take this opportunity to thank all the people that helped me during my Master thesis.

First of all, I would like to thank Prof. Dr. Jan Meijer for the given chance to dive deeper in the fascinating world of color centers in diamond research and for providing me with this interesting topic as well as for the support, knowledge and advice. Thank you to my second supervisor Dr. Sébastien Pezzagna for helping me with sample preparation and measurements, sharing the knowledge and experience as well as for the support. I would also like to give a special thank you to Tobias Lühmann, without your immense experience with the 100 keV accelerator, my work would not be possible. I am giving my thanks to the entire "Applied Quantum System Department" group for making me feel welcome and sharing your experimental tips and experience with me.

Finally, a special welcome to my family for your support, for believing in me and for encouraging me when I needed it the most.

Selbständigkeitserklärung

Hiermit erkläre ich, Ena Osmić, dass ich die vorliegende Masterarbeit selbständig verfasst und keine anderen als die angegebenen Hilfsmittel benutzt habe. Die Stellen der Masterarbeit, die anderen Quellen im Wortlaut oder dem Sinn nach entnommen wurden, sind durch Angaben der Herkunft kenntlich gemacht. Dies gilt auch für Zeichnungen, Skizzen, bildliche Darstellungen sowie für Quellen aus dem Internet. Ich versichere außerdem, dass die vorliegende Arbeit noch keinem anderen Prüfungsverfahren zugrunde gelegen hat bzw. keiner weiteren Stelle zur Prüfung vorgelegt wurde.

Leipzig, 10.05.2021

Ena Osmić